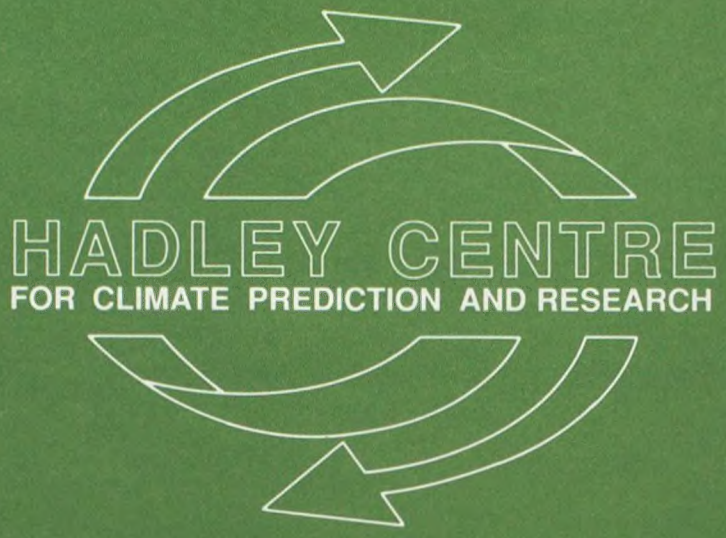

The impact of new land surface physics on the GCM simulation of climate and climate sensitivity

by

P M Cox, R A Betts, C B Bunton,
R L H Essery, P R Rowntree and J Smith

CRTN 82

March 1998

CLIMATE
RESEARCH
TECHNICAL
NOTE

Hadley Centre
Meteorological Office
London Road
Bracknell
Berkshire RG12 2SY

CLIMATE RESEARCH TECHNICAL NOTE NO. 82

THE IMPACT OF NEW LAND SURFACE PHYSICS ON THE GCM SIMULATION OF CLIMATE AND CLIMATE SENSITIVITY

by

P M Cox, R A Betts, C B Bunton, R L H Essery,
P R Rowntree and J Smith

Hadley Centre for Climate Prediction and Research
Meteorological Office
London Road
Bracknell
Berkshire RG12 2SY

NOTE: This paper has not been published. Permission to quote from it should be obtained from the Director of the Hadley Centre.

© Crown Copyright 1998

The impact of new land surface physics on the GCM simulation of climate and climate sensitivity

P.M. Cox, R.A. Betts, C.B. Bunton
R.L.H. Essery, P.R. Rowntree, J. Smith

Hadley Centre, Met Office, Bracknell, Berks RG12 2SY, UK

March 6, 1998

Abstract

Recent improvements to the Hadley Centre climate model include the introduction of a new land surface scheme called "MOSES" (Met Office Surface Exchange Scheme). MOSES is built on the previous scheme, but incorporates in addition an interactive plant photosynthesis and conductance module, and a new soil thermodynamics scheme which simulates the freezing and melting of soil water, and takes account of the dependence of soil thermal characteristics on the frozen and unfrozen components. The impact of these new features is demonstrated by comparing $1\times CO_2$ and $2\times CO_2$ climate simulations carried out using the old ("UKMO") and new ("MOSES") land surface schemes. MOSES is found to improve the simulation of current climate. Soil water freezing tends to warm the high latitude land in the northern hemisphere during autumn and winter, whilst the increased soil water availability in MOSES alleviates a spurious summer drying in the mid-latitudes. The interactive canopy conductance responds directly to CO_2, suppressing transpiration as the concentration increases and producing a significant enhancement of the warming due to the radiative effects of CO_2 alone.

1 Introduction

Land surface schemes are crucial components of Numerical Weather Prediction (NWP) and General Circulation Models (GCMs), calculating the surface to atmosphere fluxes of heat and water, and updating the surface and subsurface variables which affect these fluxes. Offline tests have demonstrated that apparently small differences amongst these schemes can lead to a wide spread in the results (Henderson-Sellers *et al* (1996)), but it is still unclear how this spread is affected by coupling the schemes to a host atmospheric model. Moreover, even less has been published concerning the impact of land surface process representation on GCM simulations of climate sensitivity to increasing greenhouse gases, which are currently the focus of so much public concern (Houghton *et al* (1995)).

The realisation that land surface schemes can influence the performance of atmospheric models has driven an increase in the complexity of these schemes. The first Numerical Weather Prediction (NWP) and General Circulation Models (GCMs) to include any treatment of land surface processes used variants of the simple "bucket" model (Carson (1982)). In these, the status of the land surface was defined in terms of the surface temperature and the soil moisture held in a single store (or bucket), surface evaporation was calculated as the product of a potential rate and a soil moisture dependent "β" factor, and runoff was assumed to occur whenever the bucket overflowed. Schemes of this type generally assumed geographically uniform values for the water holding capacity of the bucket and neglected the significant impact of vegetation and soil types on the surface to atmosphere fluxes of heat, water and momentum.

A second generation of land surface schemes were developed in the mid-eighties to address some of the obvious limitations of the bucket model (Sellers *et al* (1986)). Amongst these was a scheme of intermediate complexity developed for use in the Meteorological Office (MO) 11 layer model and later included within the Unified Model (UM) system (Warrilow and Buckley (1989)). This scheme (hereafter called the "UKMO" scheme) has performed quite well in the PILPS intercomparisons (Chen *et al* (1997)), but it includes a number of simplifications which may constrain its ability to respond realistically to extremes in meteorological and climatological forcing. A new scheme, called "MOSES" (Met Office Surface Exchange Scheme) has recently been designed to remove some of these limitations.

In addition to calculating water and energy fluxes, MOSES also calculates vegetation to atmosphere fluxes of CO_2 incorporating the direct physiological effect of atmospheric CO_2 concentrations on both photosynthesis and stomatal conductance, which may provide a significant additional climate forcing under enhanced CO_2 (Sellers *et al* (1996)). The calculation of surface CO_2 fluxes is a vital step towards the incorporation of a fully dynamic biosphere within GCM's, which would enable the full range of climate-vegetation feedbacks to be included consistently in predictions of climate change (Betts *et al* (1997)).

The next section describes MOSES, highlighting the major new features compared to the UKMO scheme. The remainder of the paper focusses on the impact of these new features on Atmospheric GCM (AGCM) simulations of the current climate ($1\times CO_2$) and a doubled CO_2 climate ($2\times CO_2$).

2 The Met Office Surface Exchange Scheme ("MOSES")

Figure 1 is a schematic representation of MOSES, in which the state of the land surface is defined in terms of lying snow mass, σ, canopy water, c, and the temperatures , T_s, and moisture contents, M, of a number of soil layers in the vertical. The canopy water is the precipitation intercepted by plant leaves which is available for free evaporation. In its standard configuration MOSES employs 4 soil layers with thicknesses from the surface downwards of 0.1, 0.25, 0.65 and 2.0 metres.

a Evaporative Fluxes

The total moisture flux from the land surface, E is made-up of evaporation from the canopy store, E_c, transpiration by vegetation , E_v, bare soil evaporation, E_b, and sublimation from the snow surface, E_σ. In this version of MOSES snow is assumed to be uniformly distributed and the evaporative demand is met by any lying snow first, so:

$$E = \begin{cases} E_v + E_b + E_c & \text{for } \sigma = 0 \\ E_\sigma & \text{for } \sigma > 0 \end{cases} \quad (1)$$

As suggested by figure 1, sublimation and local canopy evaporation are both subject to an aerodynamic resistance, r_a, but no surface resistance. However, canopy evaporation only occurs from the fraction of the gridbox, f_a, which has a wet canopy:

$$E_c = f_a \frac{\rho}{r_a} \{q_{sat}(T_*) - q_1\} \quad (2)$$

where ρ is the surface air density, q_1 is the atmospheric specific humidity and $q_{sat}(T_*)$ is the saturated specific humidity at the surface temperature, T_*. The aerodynamic resistance, r_a, depends on roughness length, windspeed and atmospheric stability. The wet fraction, f_a, is assumed to increase linearly with canopy water reaching unity at the canopy water capacity (see table 1 for typical values). Transpiration, E_v, occurs from the vegetated fraction, ν, of the remainder of the gridbox, and is subject to both the aerodynamic resistance and a canopy or "bulk stomatal" resistance, r_c:

$$E_v = (1 - f_a)\, \nu \frac{\rho}{r_a + r_c} \{q_{sat}(T_*) - q_1\} \quad (3)$$

The canopy resistance is the inverse of the canopy conductance, g_c, which is calculated within the canopy conductance and primary productivity module described in section 2c. Bare soil evaporation, E_b, occurs from the "dry canopy", non-vegetated fraction of the gridbox, dependent on a fixed soil surface resistance, r_{ss}, (set to 100 s m^{-1}) and the volumetric soil moisture concentration within the top soil layer, Θ_1:

$$E_b = (1 - f_a)\,(1 - \nu)\,\beta(\Theta_1) \frac{\rho}{r_a + r_{ss}} \{q_{sat}(T_*) - q_1\} \quad (4)$$

where

$$\beta(\Theta) = \begin{cases} 1 & \text{for } \Theta > \Theta_c \\ \dfrac{\Theta - \Theta_w}{\Theta_c - \Theta_w} & \text{for } \Theta_w < \Theta \leq \Theta_c \\ 0 & \text{for } \Theta \leq \Theta_w \end{cases} \quad (5)$$

and Θ_w and Θ_c are soil dependent parameters (see table 2).

b Surface Energy Balance

This version of MOSES does not distinguish between the temperatures of different surface types or hydrological regimes within each gridbox, so the total evaporation may simply be written as:

$$E = \psi \frac{\rho}{r_a} \{q_{sat}(T_*) - q_1\} \tag{6}$$

where the factor ψ is defined by equations 1 to 4:

$$\psi = \begin{cases} f_a + (1 - f_a)\left\{\dfrac{\nu}{1 + r_c/r_a} + \dfrac{\beta(\Theta_1)\,(1-\nu)}{1 + r_{ss}/r_a}\right\} & \text{for } \sigma = 0 \\ 1 & \text{for } \sigma > 0 \end{cases} \tag{7}$$

The sensible heat flux, H, can be written in a similar form to equation 6:

$$H = \frac{\rho c_p}{r_a}\left\{T_* - T_1 - \frac{g}{c_p} z_1\right\} \tag{8}$$

where c_p is the specific heat capacity of the air, g is the acceleration due to gravity and T_1 is the atmospheric temperature at a reference height z_1 above the surface. Energy balance at the land-atmosphere interface requires:

$$R_n = H + LE + L_f S_m + G_0 \tag{9}$$

where R_n is the net radiation at the surface, L_f is the latent heat of fusion for water and S_m is the rate of snowmelt. The ground heat flux, G_0, is the conductive flux from the surface to the centre of the top soil layer:

$$G_0 = \frac{2\lambda}{\Delta z_1}\{T_* - T_{s1}\} \tag{10}$$

where Δz_1 is the thickness of the top soil layer and T_{s1} is the first subsurface temperature. The thermal conductivity, λ, is a function of the soil moisture in both liquid and frozen forms, and is calculated according to the algorithm proposed by Farouki (1981) as described in appendix B. When snow is lying, T_{s1}, becomes the combined temperature of the snow and top soil layer, and λ is modified to take account of the insulating effects of snow (see appendix C).

In the absence of snowmelt the surface energy balance equation (9) can be used to eliminate T_* from equations 6, 8 and 10. The resulting equation for the evaporative flux is an extension of the standard Penman-Monteith formulation to include a model of conductive heat transport through the soil:

$$E = \psi \frac{\rho}{r_a} \frac{\left\{\alpha_1\left[R_n - \dfrac{2\lambda}{\Delta z_1}\left(T_1 - T_{s1} + \dfrac{g}{c_p} z_1\right)\right] + \left(\dfrac{c_p \rho}{r_a} + \dfrac{2\lambda}{\Delta z_1}\right)\left(\Delta q_1 + \alpha_1 \dfrac{g}{c_p} z_1\right)\right\}}{\left\{\dfrac{c_p \rho}{r_a} + L\alpha_1 \psi \dfrac{\rho}{r_a} + \dfrac{2\lambda}{\Delta z_1}\right\}} \tag{11}$$

where:

$$\alpha_1 = \left.\frac{dq_{sat}}{dT}\right]_{T=T_1} \tag{12}$$

$$\Delta q_1 = q_{sat}(T_1) - q_1 \tag{13}$$

Similar equations can be derived for the sensible and the ground heat fluxes. The surface temperature is a diagnostic in this formulation:

$$T_* = T_{s1} + \frac{G_0 \Delta z_1}{2\lambda} \tag{14}$$

When snow is lying, melt occurs whenever T_* or T_{s1} exceed the freezing point of water, T_m. In the former case sufficient snowmelt occurs so as to ensure that equation 9 is satisfied for $T_* = T_m$ and the other surface fluxes are adjusted appropriately.

c Canopy Conductance and Primary Productivity

This section describes the component of MOSES which simulates canopy conductance and net primary productivity (NPP). The canopy conductance represents the bulk effect of stomatal openings on plant leaves, which respond to environmental stimuli, controlling both the loss of water by transpiration (see equation 3) and the gain of carbon dioxide through photosynthesis. NPP is the net atmosphere to vegetation carbon flux which may be considered as a diagnostic of "vegetation health".

Since CO_2 must diffuse through stomata before it can be fixed by photosynthesis, there is a simple relationship between net leaf photosynthesis, A (mol CO_2 m^{-2} s^{-1}), and stomatal conductance to water vapour, g_l (m s^{-1}):

$$A = \frac{g_l}{1.6\,R\,T_*}(c_c - c_i) \tag{15}$$

where R is the perfect gas constant, T_* is the leaf surface temperature, and c_c and c_i are the leaf surface and internal CO_2 partial pressures respectively. The factor of 1.6 accounts for the different molecular diffusivities of water and carbon dioxide. Leaf photosynthesis is known to be dependent on a number of environmental variables as well as the internal CO_2 concentration, c_i:

$$A = A(\vec{X}, c_i) \tag{16}$$

where $\vec{X}$ represents a general vector of environmental variables. Equations 15 and 16 contain three unknowns; A, g_l and c_i. The closure suggested by Jacobs (1994) is adopted here:

$$\left\{\frac{c_i - \Gamma}{c_c - \Gamma}\right\} = F_0\left\{1 - \frac{D_*}{D_c}\right\} \tag{17}$$

where Γ is the internal partial pressure of CO_2 at which photosynthesis just balances photorespiration (the "photorespiration compensation point"), D_* is the humidity deficit at the leaf surface, and F_0 and D_c are vegetation specific parameters derived by calibration. The leaf photosynthesis models represented by equation 16 are derived from the work of Collatz *et al* (1991) and Collatz *et al* (1992) for C_3 and C_4 plants respectively. Details of these models are given in appendix A. An additional direct soil moisture dependence is introduced as suggested by Cox *et al* (Accepted for Publication):

$$A = A_p\,\beta(\Theta_r) \tag{18}$$

where A_p is the "potential" (non-moisture stressed) rate of net photosynthesis as given by the models of appendix A, Θ_r is the mean soil moisture concentration within the rootzone and $\beta(\Theta_r)$ is the moisture availability factor given by equation 5.

Equations 15 to 18 represent a coupled model of stomatal conductance and leaf photosynthesis. Large-scale applications require an economical means of scaling the predicted leaf-level fluxes up to the canopy scale. The approach of Sellers *et al* (1992) is used here, in which the primary determinants of photosynthesis, mean incident photosynthetically active radiation, I_{par}, and leaf nitrogen concentration, n_l (kg N (kg C)$^{-1}$), are assumed to be proportional throughout the plant canopy:

$$I_{par}(l) = I_{par}(0)\exp\{-0.5\,l\} \tag{19}$$

$$n_l(l) = n_l(0)\exp\{-0.5\,l\} \tag{20}$$

where (l) denotes values beneath l leaf layers, (0) denotes values at the top of the canopy, and 0.5 is the PAR extinction coefficient. The maximum rate of carboxylation of rubisco, V_{max}, is also assumed to be linearly dependent on the leaf nitrogen concentration, n_l, as suggested by the survey of Schulze *et al* (1994):.

$$V_{max}\,[\text{mol } CO_2\ m^{-2}\ s^{-1}] = \begin{cases} 0.0008\,n_l & \text{for } C_3 \text{ plants} \\ 0.0004\,n_l & \text{for } C_4 \text{ plants} \end{cases} \tag{21}$$

The constants of proportionality are derived from Schulze *et al* (1994) by assuming that dry matter is 40% carbon by mass and that the maximum rate of photosynthesis is approximately equal to $0.5V_{max}$ for C_3 plants and approximately equal to V_{max} for C_4 plants.

Equations 19, 20 and 21 ensure that the relative importance of each of the factors limiting photosynthesis remain the same throughout the depth of the canopy (see appendix A). As a consequence

it is straightforward to integrate the leaf conductance and photosynthesis over the canopy leaf area index, L, to yield canopy conductance, g_c, net canopy photosynthesis, A_c, and (non-moisture stressed) canopy dark respiration, R_{dc}:

$$g_c = g_l f_{par} \quad (22)$$

$$A_c = A f_{par} \quad (23)$$

$$R_{dc} = R_d f_{par} \quad (24)$$

where g_l, A and R_d are the conductance, net photosynthesis and (non-moisture stressed) dark respiration rate of the top leaf layer and

$$f_{par} = \frac{1 - \exp\{-0.5\,L\}}{0.5} \quad (25)$$

Taken together these elements yield canopy conductance and photosynthesis values which depend realistically on temperature, solar irradiance, humidity deficit, soil moisture concentration, canopy leaf area index and atmospheric CO_2 concentration (see figure 2). These response curves are dependent on the photosyntetic pathway (i.e. C_3 or C_4) and should also be dependent on plant functional type through the vegetation specific parameters F_0 and D_c. However, for the purposes of this study only two general classes of vegetation cover were distinguished by this module; predominantly forest for which $F_0 = 0.875$ and $D_c = 0.09$ kg kg^{-1}, and predominantly C_3 grassland for which $F_0 = 0.925$ and $D_c = 0.150$ kg kg^{-1}. These parameter values were chosen to give a reasonable response to humidity deficit along with a realistic maximum canopy conductance (Dolman *et al* (1991), Schulze *et al* (1994)). Leaf nitrogen concentration may also vary with soil fertility, but for simplicity we set the top-leaf value to a uniform 0.05 kg N (kg C)$^{-1}$ regardless of vegetation type. A later study will assess the sensitivity of the results to this assumption.

Gross primary productivity, Π_G, is equivalent to the gross canopy photosynthesis:

$$\Pi_G = 0.012\,\{A_c + R_{dc}\,\beta\} \quad (26)$$

where the factor 0.012 converts from units of mol CO_2 m^{-2} s^{-1} to kg C m^{-2} s^{-1}, and the second term in the brackets is the actual (moisture modified) canopy dark respiration. Net primary productivity, Π, is:

$$\Pi = \Pi_G - R_p \quad (27)$$

where plant respiration, R_p, is split into maintenance and growth respiration:

$$R_p = R_{pm} + R_{pg} \quad (28)$$

Growth respiration is assumed to be 25% of gross photosynthesis minus maintenanence respiration:

$$R_{pg} = 0.25\,\{\Pi_G - R_{pm}\} \quad (29)$$

and therefore also a fixed fraction (0.33) of net primary productivity. Leaf maintenance respiration is equivalent to the moisture modified canopy dark respiration, βR_{dc}, while root and stem respiration is assumed to be independent of soil moisture, but to have the same dependences on nitrogen content and temperature. Thus total maintenance respiration is given by:

$$R_{pm} = 0.012\,R_{dc}\left\{\beta + \frac{(N_r + N_s)}{N_l}\right\} \quad (30)$$

where N_l, N_s and N_r are the total nitrogen contents of leaf, stem and root. The nitrogen contents of leaf and root are taken to be equal and given by:

$$N_l = 0.04\,\bar{n_l}\,L \quad (31)$$

where $\bar{n_l}$ is the mean leaf nitrogen concentration, L is the canopy leaf area index and the factor of 0.04 represents an assumed specific leaf density in kg C m^{-2}. Stem nitrogen concentration is a prescribed fraction, μ_{sl}, of the mean leaf nitrogen concentration, so:

$$N_s = \mu_{sl}\,\bar{n_l}\,S \quad (32)$$

where S is the carbon content of the respiring stem. In this study $\mu_{sl} = 0.04$ for forests and $\mu_{sl} = 1$ for grasslands. The respiring stemwood is calculated using a "pipemodel" approach in which live stemwood is proportional to the product of leaf area and canopy height (Friend *et al* (1993)):

$$S = 0.01\,h\,L \quad (33)$$

d Soil Thermodynamics and Soil Water Phase Change

As in the UKMO land surface scheme subsurface temperatures are updated using a discretised form of the heat diffusion equation. However, the MOSES module includes two significant new features. Firstly, the soil thermal characteristics are realistic functions of soil moisture content (liquid water and ice) rather than soil specific constants. Secondly, soil water phase changes are simulated and the associated latent heat is included in the subsurface calculations.

The temperature of the n^{th} soil layer, of thickness Δz_n, is incremented by the diffusive heat fluxes into and out of the layer, G_{n-1} and G_n respectively, and the net heat flux, J_n, advected from the layer by the moisture flux:

$$C_A \, \Delta z_n \frac{dT_{sn}}{dt} = G_{n-1} - G_n - J_n \, \Delta z_n \tag{34}$$

The diffusive and advective fluxes are given by:

$$G = \lambda \frac{\partial T}{\partial z} \tag{35}$$

$$J = c_w W \frac{\partial T}{\partial z} \tag{36}$$

where z is the vertical coordinate, W is the vertical flux of soil moisture (calculated within the soil hydrology module), c_w is the specific heat capacity of water, and λ is the local soil thermal conductivity (see appendix B), modified in the presence of lying snow (see appendix C) . The "apparent" volumetric heat capacity of the layer, C_A, is given by:

$$C_A = C_s + \rho_w c_w \Theta_u + \rho_i c_i \Theta_f + \rho_w \{(c_w - c_i)T + L_f\} \frac{\partial \Theta_u}{\partial T} \tag{37}$$

where Θ_u and Θ_f are the volumetric concentrations of frozen and unfrozen soil moisture, and ρ_i and c_i are the density and specific heat capacity of ice. The first three terms on the righthandside of equation 37 represent contributions from dry soil, liquid water and ice, and the final term is the apparent heat capacity associated with phase change. The relationship between unfrozen water concentration, Θ_u, and temperature, T, can be derived by minimising the Gibbs free energy of the soil-water-ice system (Williams and Smith (1989)). This results in an equation relating the water suction , Ψ (m), to the temperature, T (K), when ice is present (Miller (1965), Black and Tice (1988)):

$$\Psi = -k \left\{ \frac{\rho_i}{\rho_w} \frac{L_f}{T_m g} \right\} (T - T_m) \tag{38}$$

where T_m (K) is the freezing point of pure water, g is the acceleration due to gravity and k is a dimensionless constant which depends on the nature of the soil. A value of $k = 1.0$ is assumed, which is consistent with a clay-rich soil for which absorption forces dominate over capilliary forces. ($k = 2.2$ would be more appropriate for granular soils (Black and Tice (1988))). Combining equation 38 with the Clapp and Hornberger (1978) form (equation 53) for the suction as a function of liquid water yields:

$$\frac{\Theta_u^{max}}{\Theta_s} = \left\{ -\frac{\kappa(T - T_m)}{\Psi_s} \right\}^{-1/b} \tag{39}$$

where Θ_u^{max} is the maximum unfrozen water that can exist at temperature T, Θ_s is the saturation soil moisture concentration, Ψ_s and b are other soil specific parameters (see table 2) and κ is a constant defined by:

$$\kappa = k \frac{\rho_i}{\rho_w} \frac{L_f}{g T_m} \approx 114.3 \quad \mathrm{m\ K^{-1}} \tag{40}$$

Figure 3(a) plots Θ_u^{max} versus temperature, and figures 3(b) and 3(c) show corresponding curves for the apparent heat capacity and effective soil thermal conductivity. The actual value of Θ_u is limited by the total water content of the soil:

$$\Theta_u = \min \{\Theta_u^{max}, \Theta\} \tag{41}$$

where Θ is the "liquid" total volumetric concentration, i.e. that which would arise if all the moisture was in liquid form:

$$\Theta = \Theta_u + \frac{\rho_i}{\rho_w}\Theta_f \tag{42}$$

The temperature above which all soil moisture is unfrozen, T_{max}, can be derived by equating Θ to Θ_u^{max} in equation 39:

$$T_{max} = T_m - \frac{\Psi_s}{\kappa}\left\{\frac{\Theta_s}{\Theta}\right\}^b \tag{43}$$

The second term on the righthandside represents the suppression of the initial freezing point. It is useful to rewrite equation 41 in terms of two distinct temperature regimes:

$$\Theta_u = \begin{cases} \Theta_u^{max} & \text{if } T < T_{max} \\ \Theta & \text{if } T \geq T_{max} \end{cases} \tag{44}$$

then differentiation with respect to temperature yields:

$$\frac{\partial \Theta_u}{\partial T} = \begin{cases} \dfrac{\kappa\Theta_s}{b\Psi_s}\left\{-\dfrac{\kappa(T-T_m)}{\Psi_s}\right\}^{(-1/b-1)} & \text{if } T < T_{max} \\ 0 & \text{if } T > T_{max} \end{cases} \tag{45}$$

which is used in equation 37. The surface soil heat flux, G_0, is provided by the surface and boundary layer model as the residual of the surface energy balance:

$$G_0 = R_n - H - LE - L_f S_m \tag{46}$$

where R_n is the net radiation at the surface, H and LE are the surface sensible and latent heat fluxes respectively and S_m is the rate of snowmelt. Heat advection by surface infiltration is currently neglected. The lower boundary condition corresponds to zero vertical gradient in soil temperature.

e Soil Hydrology

The soil hydrology component of MOSES is based on a a finite difference approximation to the Richards' equation (Richards (1931)), with the same vertical discretisation as the MOSES soil thermodynamics module. The prognostic variables of the model are the total soil moisture contents within each layer:

$$M = \rho_w \Delta z \Theta_s \{S_u + S_f\} \tag{47}$$

where Δz is the thickness of the layer, and S_u and S_f are the mass of unfrozen and frozen water within the layer as a fraction of that of liquid water at saturation:

$$S_u = \frac{\Theta_u}{\Theta_s} \tag{48}$$

$$S_f = \frac{\rho_i}{\rho_w}\frac{\Theta_f}{\Theta_s} \tag{49}$$

The total soil moisture content within the n^{th} soil layer is incremented by the diffusive water flux flowing in from the layer above, W_{n-1}, the diffusive flux flowing out to the layer below, W_n, and the evapotranspiration extracted directly from the layer by plant roots, E_n:

$$\frac{dM_n}{dt} = W_{n-1} - W_n - E_n \tag{50}$$

The water fluxes are given by the Darcy equation:

$$W = K\left\{\frac{\partial \Psi}{\partial z} + 1\right\} \tag{51}$$

where K is the hydraulic conductivity and Ψ is the soil water suction. To close the model it is necessary to assume forms for the hydraulic conductivity and the soil water suction as a function of the soil moisture concentration. The dependencies suggested by Clapp and Hornberger (1978) are most often used in GCM land-surface schemes, primarily because of their relative simplicity. In addition the work of Cosby *et al* (1984) offers a means of linking the parameters which define these curves to soil particle size distribution. More sophisticated dependencies, such as those derived by van Genuchten *et al* (1991), are probably not justified in large-scale models because of the uncertainties associated with heterogeneity and non-Darcian flow. For these reasons the Clapp and Hornberger relations are also used in MOSES:

$$\Psi = \Psi_s S_u^{-b} \tag{52}$$

$$K = K_s S_u^{2b+3} \tag{53}$$

where K_s, Ψ_s and b are empirical soil dependent constants. The interpretation of the Clapp-Hornberger relations in terms of unfrozen rather than total soil moisture is consistent with the observation that the freezing of soil moisture reduces hydraulic conductivity and produces a large suction by reducing the unfrozen water content (Williams and Smith (1989)).

The fraction of the transpiration, e_n, which is extracted from each of the soil layers within the rootdepth is assumed to be equal to the fraction of the total available soil moisture provided by that layer:

$$e_n = \frac{\Delta z_n \left(\Theta_u(n) - \Theta_w\right)}{\sum_{n_r} \Delta z_n \left(\Theta_u(n) - \Theta_w\right)} \tag{54}$$

where $\Theta_u(n)$ is the volumetric concentration of unfrozen water within the n^{th} layer and Θ_w is the wilting point appropriate to the soil type (see table 2). The number of layers accessed by the plant roots, n_r, is taken to be 3 for grasslands (corresponding to a rootdepth of 1 metre) and 4 for forests (corresponding to a rootdepth of 3 metres). Bare soil extraction is taken directly from the top soil layer, so the sink term in equation 50 becomes:

$$E_n = \begin{cases} E_b + e_1 E_v & \text{for } n = 1 \\ e_n E_v & \text{for } n > 1 \end{cases} \tag{55}$$

The top boundary condition for the MOSES soil hydrology module is:

$$W_0 = P_f + S_m - Y_s \tag{56}$$

where W_0 is the flux which infiltrates at the surface and S_m, P_f, and Y_s are the fluxes of snowmelt, throughfall precipitation, and surface runoff respectively. Surface runoff occurs when the the local water flux at the soil surface exceeds the saturated hydraulic conductivity. An exponential sub-grid distribution of rainfall intensities is assumed in order to calculate gridbox mean values of surface runoff and canopy throughfall in the manner described by Dolman and Gregory (1992). The default lower boundary condition corresponds to "free drainage":

$$W_N = K_N \tag{57}$$

where W_N is the drainage from the lowest deepest soil layer and K_N is the hydraulic conductivity of this layer.

f Surface Parameters

Aside from the internal canopy conductance parameters described in section 2c and the mean vegetated fraction of the gridbox, ν, MOSES requires 8 soil dependent and 7 vegetation dependent parameters. Geographically varying fields of the vegetation parameters are derived by assigning typical values to the 23 land cover classes of the Wilson and Henderson-Sellers (1985) land-cover dataset (see table 1). The scheme simulates just a single surface type within each gridbox so effective parameters must

be derived for each point. These are taken as the area-weighted mean for all parameters but the roughness length, which is aggregated using a blending height approach (Mason (1988)).

Effective values for the soil parameters are calculated from the gridbox mean fractions of sand, silt and clay using the regression technique of Cosby *et al* (1984). The sand, silt and clay values are area-weighted means derived by assigning typical fractions to the 3 soil textural classes distinguished within the Wilson and Henderson-Sellers (1985) dataset. These fractions are shown in table 2 along with the resulting soil parameters.

g Summary of Differences between MOSES and the UKMO Scheme

The original UKMO scheme was used in version 2 of the Hadley Centre Coupled Model (HadCM2) as described by Johns *et al* (1997). In this scheme the hydrological state of the land surface is defined by 3 variables; available soil moisture, lying snow and canopy water. The soil moisture store has a depth equal to the gridbox mean rootdepth which is up to 50% smaller than in MOSES, varying from about 0.5 metres for grasslands to 1.5 metres for tropical forests. As with MOSES, the soil heat flux is calculated using a vertically discretised heat diffusion equation with 4 soil layers, but soil water phase change effects are ignored. The partitioning of the net radiation into latent and sensible heat components is based on an Ohm's law anologue, but the surface temperature is taken to be equal to the top soil layer temperature, rather than being diagnosed from a Penman-Monteith type surface energy balance. Evapotranspiration from the soil is limited directly by moisture availability and is subject to a non-interactive gridbox mean surface resistance, like bare soil evaporation in MOSES (equation 4).

A 4-layer soil hydrology model, based on a discretised form of Richards' equation (Richards (1931)) and utilising the soil water suction and hydraulic conductivity curves given by van Genuchten *et al* (1991), was introduced as an option in later versions of the model. Effective parameters for these curves were derived as area-weighted means of parameters assigned to each of the Wilson and Henderson-Sellers (1985) soil texture classes present in each gridbox. The impact of this change alone was found to have a negligible impact on the GCM climatology, but it is this more recent variant of the UKMO scheme which has been used in this study. The differences between this scheme and MOSES are summarised in table 3.

3 GCM Climate Simulations

a Methodology for GCM Climate Simulations

A series of fixed-SST ("timeslice") GCM experiments were carried out to assess the impact of MOSES on the simulation of the current climate and the climate sensitivity to CO_2. The experiments used the atmosphere-land component of version 3 of the Hadley Centre Climate Model (HadAM3, Pope *et al* (In preparation)), which is the latest climate version of the UK Meteorological Office Unified Model (Cullen (1993)). The model dynamics use a split-explicit finite difference scheme on an Arakawa 'B' grid in the horizontal and hybrid vertical coordinates (sigma or pressure normalised by surface pressure in the lower layers changing smoothly to pressure above about 50hPa). This climate version has a horizontal resolution of 2.5° latitude by 3.75° longitude, and has 19 atmospheric layers. Major changes from earlier versions include a new radiation scheme (Edwards and Slingo (1996)), and a parametrization of momentum transfer by convective processes (Kershaw and Gregory (1997)). Full details and the performance of the model are described by Pope *et al* (In preparation).

The simulations of current climate were carried out using prescribed climatological monthly mean sea-surface temperatures and sea-ice extents derived over the period from 1979 to 1988, as defined for the Atmospheric Model Intercomparison Project (AMIP, Slingo *et al* (1996)). The $2\times CO_2$ simulations utilised anomalies in sea-surface temperatures and sea-ice extents as simulated in the Hadley Centre's 2nd transient climate change experiment for the 20 years around the time of CO_2 doubling (Mitchell *et al* (1995)). Each of the simulations were carried out for 15 model years, and climatological means were derived from the last 10 years to avoid any spin-up effects.

A set of seven simulations were carried out to isolate the impacts of each new element of MOSES:

(i) $1\times CO_2$, UKMO

(ii) $1\times CO_2$, MOSES

(iii) $1\times CO_2$, MOSES without soil water freezing

(iv) $2\times CO_2$, UKMO

(v) $2\times CO_2$, MOSES

(vi) $2\times CO_2$, MOSES without soil water freezing

(vii) $2\times CO_2$, MOSES without direct CO_2 effect

b Impact on the Simulation of Current Climate

Figure 4 shows the error in screen level temperature relative to the Legates and Willmott climatology (Legates and Willmott (1990)) for the $1\times CO_2$ UKMO simulation. Temperatures are underestimated over land in the northern hemisphere winter (figure 4(a)) and overestimated in mid-latitudes in summer (figure 4(b)). The latter is associated with drying of the soil and a subsequent feedback on cloud and precipitation.

MOSES has a beneficial impact on both of these errors. Figure 5 shows the difference in screen level temperature simulated in the $1\times CO_2$ MOSES and UKMO simulations. The inclusion of soil water phase change tends to warm the high latitudes in autumn and winter (figure 5(a)), whilst increased water availability, primarily as a result of the increased rootdepths, allows evaporative cooling to be maintained throughout the summer in the mid-latitudes (figure 5(b)). Overall, MOSES has a neutral impact on the quality of the GCM simulation of precipitation over land, but provides a significant improvement in the RMS screen level temperature errors (see table 4).

The improvement is particularly marked in Europe, where the deficiency in summer precipitation (figure 6(b)) and associated overestimate of mean temperatures (figure 6(a)) is almost removed. This is a combined result of the increased rootdepths and the inclusion of soil water phase change. The increased rootdepths allow more moisture to be stored in the soil in spring, so that a longer period of net drying can be maintained before evaporation becomes water limited (figure 6(e)). Frozen soil water in the northern areas of the region is unable to drain but augments the available soil moisture when it melts in spring. Both of these effects act to increase evaporation (figure 6(c)), cloud cover and precipitation (figure 6(b)) in summer.

c Impact on the Climate Sensitivity to Doubling CO_2

Table 5 shows the sensitivity of the climate over land to doubling CO_2 for the runs carried out with (a) the UKMO scheme ; (b) MOSES; (c) MOSES without soil freezing and (d) MOSES without the direct CO_2 effect on plants. MOSES increases the mean warming over land from 3.18K to 3.45K. This is mostly due to the direct effect of CO_2 on stomatal conductance, which acts to suppress evaporation, reduce cloud cover and increase near surface temperatures. The climate simulations which exclude this effect predict increased evaporation from land under doubled CO_2 (table 5(a) and 5(d)), whilst those which include it show reductions (5(b) and 5(c)).

Figure 7 shows the geographical pattern of the changes in climate sensitivity which result from changing the land surface scheme alone. These maps were calculated by subtracting the climate sensitivity simulated with the UKMO scheme from that simulated with MOSES. MOSES is seen to reduce the warming over North America in winter (figure 7(a)) but markedly increases the year-round sensitivity of Amazonia (7(a) and 7(b)). The additional warming in Amazonia is a consequence of reduced evaporation arising from an almost 50% reduction in canopy conductance, as can be seen from figure 8. This is mostly as a result of the direct CO_2 effect, but also has a component due to the climate change alone (dashed lines).

MOSES increases the tendency for drying of the soil (figure 9(e)) and reductions in precipitation (figure 9(b)) over Europe during summer under $2\times CO_2$. This is related to the inclusion of soil freezing (comparing dashed and dot-dash lines), and is not alleviated by CO_2-induced suppression of transpiration (comparing dashed and dot-dot-dot-dash lines). It should be noted however that the MOSES $2\times CO_2$ climate over Europe still has a more vigorous hydrological cycle than the UKMO $2\times CO_2$ climate. The differences in sensitivity are mostly a result of differences in the $1\times CO_2$ control climates (as shown in Figure 6).

d Simulated Carbon Fluxes

The coupled canopy conductance and photosynthesis module of MOSES also simulates vegetation to atmosphere fluxes of carbon as described in section 2c. Table 6 shows mean values over land from the $1\times CO_2$ MOSES simulation, the $2\times CO_2$ MOSES simulation and the $2\times CO_2$ MOSES simulation excluding the direct CO_2 effect on plants. The annual mean present-day net primary productivity (NPP) is equivalent to about 65 Gt C yr^{-1} when integrated over the entire land surface, which is close to other recent estimates (Warnant *et al* (1994)). Doubling CO_2 is simulated to reduce the diurnal mean canopy conductance by 41% and increase net primary productivity by 46%. This reduction in canopy conductance is larger than that modelled by Sellers *et al* (1996), but close to the value suggested by Morison (1987) and well within the observed range reported by Field *et al* (1995). The changes in canopy conductance and NPP are mostly attributable to the direct effect of CO_2 on vegetation, as can be seen by comparing table 6(a) and 6(c). Climate change alone results in a slight reduction in canopy conductance (-2.5%) but a more sizeable reduction in NPP (-13%).

Figure 10 shows zonal mean canopy conductance and net primary productivity from the MOSES simulations. The seasonality in both of these variables is very apparent, with northern hemisphere peaks clear in the June-July-August season but absent in the December-January-February mean. The CO_2 induced reduction in canopy conductance is also obvious (comparing continuous and dashed lines) especially in the productive tropical regions.

4 Conclusions

This paper has demonstrated that the treatment of land surface physics within GCM's can have a significant impact on the simulation of climate and climate sensitivity to atmospheric CO_2.

A new land surface scheme called "MOSES" has been shown to improve aspects of the GCM simulation of current climate. The inclusion of soil water phase change acts to warm the high northern latitudes in winter and autumn, whilst increased soil water availability (primarily as a result of increased rootdepths) prevents a spurious drying and warming in the mid-latitudes during summer.

The new land-surface physics also impacts on the sensitivity of the GCM climate to doubling atmospheric CO_2. Stomatal closure suppresses land evaporation and increases runoff under enhanced CO_2. The resulting change in surface energy partitioning produces an appreciable magnification of the warming over tropical rainforests.

The tendency of mid-latitude summer soil moisture to dry under $2\times CO_2$ was also found to be dependent on the land surface scheme employed. Reductions in available soil moisture and evaporation were more significant for MOSES than for the previous "UKMO" scheme, but its $2\times CO_2$ climate over Europe retained the more vigorous hydrological cycle as a result of larger differences in the $1\times CO_2$ control states.

Acknowledgements

The authors of this work were supported by the CEC Climate and Environment Programme under contract PL950189 (Peter Rowntree and Cyndy Bunton), the UK DETR Climate Prediction Programme under contract PECD 7/12/37 (Peter Cox, Richard Betts and Richard Essery) and the Public Meteorological Service Research and Development Programme (Jenny Smith).

References

Betts, R. A., P. M. Cox, S. E. Lee, and F. I. Woodward, 1997: Contrasting physiological and structural vegetation feedbacks in climate change simulations. *Nature*, **387**, 796–799.

Black, P. B., and R. A. Tice, 1988: Comparison of soil freezing curve and soil water curve data for windsor sandy loam. *US Army Cold Regions Research and Engineering Report,*, **88**, 16.

Carson, D. J., 1982: Current parameterisations of land-surface processes in atmospheric general circulation models. *Land Surface Processes in Atmospheric General Circulation Models*, Eagleson, P. S., Ed., Cambridge University Press.

Chen, T. H., A. Henderson-Sellers, P. C. D. Milly, A. J. Pitman, A. C. M. Beljaars, J. Polcher, F. Abramapoulos, A. Boone, S. Chang, F. Chen, Y. Dai, C. E. Desborough, R. E. Dickenson, L. Dumenil, M. Ek, J. R. Garrat, N. Gedney, Y. M. Gusev, J. Kim, R. Koster, E. A. Kowalczyk, K. Laval, J. Lean, D. Lettenmaier, X. Liang, J. F. Mahfouf, H. T. Mengelkamp, K. Mitchell, O. N. Nasonova, J. Noilhan, A. Robock, C. Rosenzweig, J. Schaake, C. A. Schlosser, J. P. Schulz, Y. Shao, A. B. Schmakin, D. L. Verseghy, P. Wetzel, E. F. Wood, Y. Xue, Z. L. Yang, and Q. Zeng, 1997: Cabauw experimental results from the Project for Intercomparison of Land-surface Parameterization Schemes (PILPS). *Journal of Climate*, **10**, 1194–1215.

Clapp, R., and G. Hornberger, 1978: Empirical equations for some soil hydraulic properties. *Water Resources Research*, **14**, 601–604.

Collatz, G. J., J. T. Ball, C. Grivet, and J. A. Berry, 1991: Physiological and environmental regulation of stomatal conductance, photosynthesis and transpiration: a model that includes a laminar boundary layer. *Agricultural and Forest Meteorology*, **54**, 107–136.

——, M. Ribas-Carbo, and J. A. Berry, 1992: A coupled photosynthesis-stomatal conductance model for leaves of C_4 plants. *Australian Journal of Plant Physiology*, **19**, 519–538.

Cosby, B. J., G. M. Hornberger, R. B. Clapp, and T. R. Ginn, 1984: A statistical exploration of the relationships of soil moisture characteristics to the physical properties of soils. *Water Resources Research*, **20**, 682–690.

Cox, P. M., C. Huntingford, and R. J. Harding, Accepted for Publication: A canopy conductance and photosynthesis model for use in a GCM land surface scheme. *Journal of Hydrology*.

Cullen, M. J. P., 1993: The unified forecast/climate model. *Meteorological Magazine*, **122**, 81–94.

Dolman, A. J., and D. Gregory, 1992: The parametrization of rainfall interception in GCMs. *Quarterly Journal of the Royal Meteorological Society*, **118**, 455–469.

Dolman, A., J. Gash, J. Roberts, and W. Shuttleworth, 1991: Stomatal and surface conductance of tropical rainforest. *Agricultural and Forest Meteorology*, **54**, 303–318.

Edwards, J., and A. Slingo, 1996: Studies with a flexible new radiation code. I: Choosing a configuration for a large-scale model. *Quarterly Journal of the Royal Meteorological Society*, **122**, 689–720.

Farouki, O., 1981: The thermal properties of snow in cold regions. *Cold Regions Science and Technology*, **5**, 67–75.

Field, C., R. Jackson, and H. Mooney, 1995: Stomatal responses to increased CO2: implications from the plant to the global scale. *Plant, Cell and Environment*, **18**, 1214–1225.

Friend, A. D., H. H. Shugart, and S. W. Running, 1993: A physiology-based model of forest dynamics. *Ecology*, **74**, 797–797.

Henderson-Sellers, A., K. McGuffie, and A. Pitman, 1996: The project for intercomparison of land-surface parametrization schemes (PILPS): 1992-1995. *Climate Dynamics*, **12**(12), 849–859.

Houghton, J. T., L. G. M. Filho, B. A. Callander, N. Harris, A. Kattenberg, and K. M. (eds), 1995: *Climate Change 1995*. Cambridge University Press.

Jacobs, C., 1994: *Direct impact of atmospheric CO_2 enrichment on regional transpiration*. PhD thesis, Wageningen Agricultural University.

Johns, T. C., R. E. Carnell, J. F. Crossley, J. M. Gregory, J. F. B. Mitchell, C. A. Senior, S. F. B. Tett, and R. A. Wood, 1997: The second Hadley Centre coupled ocean-atmosphere GCM: Model description, spinup and validation. *Climate Dynamics*, **13**, 103–134.

Kershaw, R., and D. Gregory, 1997: Parametrization of momentum transport by convection. Part I. Theory and cloud modelling results. *Quarterly Journal of the Royal Meteorological Society*, **123**(541), 1133–1151.

Legates, D. R., and C. J. Willmott, 1990: Mean seasonal and spatial variability in global surface air temperature. *Theoretical and Applied Climatology.*, **41**, 11–21.

Mason, P., 1988: The formation of areally-averaged roughness lengths. *Quarterly Journal of the Royal Meteorological Society*, **114**, 399–420.

Miller, R., 1965: Phase equilibria and soil freezing. *Permafrost:Proceedings of the Second International Conference*, National Research Council Publication 1287, Washington D.C.: National Academy of Sciences, 193–197.

Mitchell, J. F. B., T. C. Johns, J. M. Gregory, and S. F. B. Tett, 1995: Climate response to increasing levels of greenhouse gases and sulphate aerosols. *Nature*, **376**, 501–504.

Morison, J., 1987: Intercellular CO2 concentration and stomatal response to CO2. *Stomatal Function*, Zeiger, E., G. Farquhar, and I. Cowan, Eds., Stanford University Press, 229–252.

Richards, L., 1931: Capilliary conduction of liquids through porous mediums. *Physics*, **1**, 318–333.

Schulze, E. D., F. M. Kelliher, C. Korner, and J. Lloyd, 1994: Relationships among maximum stomatal conductance, ecosystem surface conductance, carbon assimilation rate, and plant nitrogen nutrition: a global ecology scaling exercise. *Annual Review of Ecological Systems*, **25**, 629–660.

Sellers, P. J., Y. Mintz, Y. C. Sud, and A. Dalcher, 1986: A simple biosphere model (SiB) for use within general circulation models. *Journal of Atmospheric Science*, **43**, 505–531.

Sellers, P., J. Berry, G. Collatz, C. Field, and F. Hall, 1992: Canopy reflectance, photosynthesis and transpiration, III. a reanalysis using enzyme kinetics - electron transport models of leaf physiology. *Remote Sensing of Environment*, **42**, 187–216.

Sellers, P. J., L. Bounoua, G. J. Collatz, D. A. Randall, D. A. Dazlich, S. O. Los, J. A. Berry, I. Fung, C. J. Tucker, C. B. Field, and T. G. Jensen, 1996: Comparison of radiative and physiological effects of doubled atmospheric CO_2 on climate. *Science*, **271**, 1402–1406.

Slingo, J. M., K. R. Sperber, J. S. Boyle, J. P. Ceron, M. Dix, B. Dugas, W. Ebisuzaki, J. Fyfe, D. Gregory, J. F. Gueremy, J. Hack, A. Harzallah, P. Inness, A. Kitoh, W. K. M. Lau, B. McAvaney, R. Madden, A. Matthews, T. N. Palmer, C. K. Park, D. Randall, and N. Renno, 1996: Intraseasonal oscillations in 15 atmospheric general circulation models: results from an AMIP diagnostic subproject. *Climate Dynamics*, **12**, 325–357.

van Genuchten, M., F. Leij, and S. Yates, 1991: The RETC code for quantifying the hydraulic functions of unsaturated soils. Technical Report EPA/600/2-91/065, U.S. Environmental Protection Agency.

Warnant, P., L. Francois, D. Strivay, and J.-C. Gerard, 1994: CARAIB: A global model of terrestrial biological productivity. *Global Biogeochemical Cycles*, 8(3), 255–270.

Warrilow, D. A., and E. Buckley, 1989: The impact of land surface processes on the moisture budget of a climate model. *Annales Geophysic e*, **7**, 439–450.

Williams, P., and M. Smith, 1989: *The Frozen Earth*. Cambridge University Press.

Wilson, M. F., and A. Henderson-Sellers, 1985: A global archive of land cover and soils data for use in general circulation climate models. *Journal of Climatology*, **5**, 119–143.

A Leaf Photosynthesis Models

The C_3 and C_4 photosynthesis models are derived from the work of Collatz *et al* (1991) and Collatz *et al* (1992). In both cases the rate of gross leaf photosynthesis, W, is calculated in terms of three potentially limiting factors:

(i) W_c represents the rate of gross photosynthesis when the photosynthetic enzyme system (RuBP) is limiting:

$$W_c = \begin{cases} V_m \left\{ \dfrac{c_i - \Gamma}{c_i + K_c\,(1 + O_a/K_o)} \right\} & \text{for } C_3 \text{ plants} \\ V_m & \text{for } C_4 \text{ plants} \end{cases} \tag{58}$$

where V_m is the maximum rate of carboxylation of Rubisco, O_a is the atmospheric partial pressure of oxygen, K_c and K_o are Michaelis-Menten constants for CO_2 and O_2 respectively, and Γ is the photorespiration compensation point.

(ii) W_l is the light-limited rate of gross photosynthesis:

$$W_l = \begin{cases} 0.068\,I_{par} \left\{ \dfrac{c_i - \Gamma}{c_i + 2\Gamma} \right\} & \text{for } C_3 \text{ plants} \\ 0.0332\,I_{par} & \text{for } C_4 \text{ plants} \end{cases} \tag{59}$$

where I_{par} is the incident photosynthetically active radiation (mol PAR photons $m^{-2}\,s^{-1}$) and the numerical factors depend on the assumed "quantum efficiency" and the leaf scattering coefficient for PAR.

(iii) W_e is the limitation associated with transport of the photosynthetic products for C_3 plants, but is the PEP-Carboxylase limitation for C_4 plants (Collatz *et al* (1992)):

$$W_e = \begin{cases} 0.5\,V_m & \text{for } C_3 \text{ plants} \\ 2 \times 10^4\,V_m \dfrac{c_i}{p_*} & \text{for } C_4 \text{ plants} \end{cases} \tag{60}$$

where p_* is the surface air pressure.

The actual rate of gross photosynthesis, W, is calculated as the smoothed minimum of these three limiting rates:

$$\beta_1 W_p^2 - W_p\,\{W_c + W_l\} + W_c W_l = 0 \tag{61}$$

$$\beta_2 W^2 - W\,\{W_p + W_e\} + W_p W_e = 0 \tag{62}$$

where W_p is the smoothed minimum of W_c and W_l, and β_1 and β_2 are "co-limitation" coefficients. The smallest root of each quadratic is selected. Finally (non-moisture stressed) net leaf photosynthesis, A_p, is calculated by subtracting the rate of dark respiration, R_d, from the gross photosynthetic rate, W:

$$A_p = W - R_d \tag{63}$$

The rate of dark respiration is assumed to be a constant fraction of the maximum rate of carboxylation of Rubisco:

$$R_d = \begin{cases} 0.015\,V_m & \text{for } C_3 \text{ plants} \\ 0.025\,V_m & \text{for } C_4 \text{ plants} \end{cases} \tag{64}$$

The internal parameters V_m, K_o, K_c and Γ are all temperature dependent functions taken from Collatz *et al* (1991) for C_3 plants and Collatz *et al* (1992) for C_4 plants.

(i) V_m, the maximum rate of carboxylation of Rubisco:

$$V_m = \begin{cases} \dfrac{V_{max}\, f_T(2.0)}{[1+\exp\{0.3\,(T_c-36)\}]} & \text{for } C_3 \text{ plants} \\ \dfrac{V_{max}\, f_T(2.0)}{[1+\exp\{0.3\,(T_c-36)\}]\,[1+\exp\{0.3\,(13-T_c)\}]} & \text{for } C_4 \text{ plants} \end{cases} \tag{65}$$

where T_c is the leaf temperature in °C, and f_T is the standard "Q10" temperature dependence:

$$f_T(q_{10}) = q_{10}^{0.1\,(T_c-25)} \tag{66}$$

(ii) Γ, the photorespiration compensation point:

$$\Gamma = \begin{cases} \dfrac{O_a}{2\,\tau} & \text{for } C_3 \text{ plants} \\ 0 & \text{for } C_4 \text{ plants} \end{cases} \tag{67}$$

where τ is the Rubisco specificity for CO_2 relative to O_2:

$$\tau = 2600\, f_T(0.57) \tag{68}$$

(iii) K_c and K_o, Michaelis-Menten constants for CO_2 and O_2:

$$K_c = 30\, f_T(2.1) \tag{69}$$

$$K_o = 3\times 10^4\, f_T(1.2) \tag{70}$$

B Effective Thermal Conductivity

The effective soil thermal conductivity, λ_s, is calculated using the algorithm proposed by Farouki (1981). In this model, the conductivity varies linearly with total moisture content:

$$\lambda_s = \{\lambda_{sat} - \lambda_{dry}\}\,\frac{\Theta}{\Theta_s} + \lambda_{dry} \tag{71}$$

where Θ is the "liquid" total volumetric concentration as given by equation 42 and Θ_s is the volumetric moisture concentration at saturation. The conductivities of dry soil, λ_{dry}, and saturated soil, λ_{sat}, are calculated as the geometric means of the conductivities of their constituents:

$$\lambda_{dry} = \lambda_m^{(1-\Theta_s)}\,\lambda_a^{\Theta_s} \tag{72}$$

$$\lambda_{sat} = \lambda_m^{(1-\Theta_s)}\,\lambda_w^{\Theta_u^s}\,\lambda_i^{\Theta_s-\Theta_u^s} \tag{73}$$

where λ_m, λ_a, λ_w and λ_i are the thermal conductivities of minerals, air, water and ice respectively, and Θ_u^s is the saturation concentration of liquid water for the current liquid water to ice mass ratio:

$$\Theta_u^s = \Theta_s\,\frac{S_u}{S_u+S_f} \tag{74}$$

Equations 72 and 73 may be combined to give λ_{sat} in terms of λ_{dry}:

$$\lambda_{sat} = \lambda_{dry}\left\{\frac{\lambda_w^{\Theta_u^s}\,\lambda_i^{\Theta_s-\Theta_u^s}}{\lambda_a^{\Theta_s}}\right\} \tag{75}$$

Values of the thermal conductivities of air, water and ice are taken from page 90 of Williams and Smith (1989):

$$\lambda_a = 0.025 \quad \mathrm{W\ m^{-1}\ K^{-1}}$$

$$\lambda_w = 0.56 \quad \mathrm{W\ m^{-1}\ K^{-1}}$$

$$\lambda_i = 2.24 \quad \mathrm{W\ m^{-1}\ K^{-1}}$$

Values of λ_{dry} are calculated offline based on soil texture. Typical values are included in table 2.

C Snow Processes

The presence of snow lying on the ground modifies the land-atmosphere interaction in a number of crucial ways. Snow provides a free source of water for sublimation, and the latent heat associated with melt is often a significant portion of the surface energy balance. However, snow also modifies surface radiative, turbulent and ground heat fluxes by making surfaces brighter and smoother, and by insulating the soil from the atmosphere. Each of these effects is represented to some extent within MOSES.

The gridbox mean surface albedo is assumed to vary from its snow-free value, α_0, in the absence of snow, to its deep-snow (temperature dependent) value of α_{sT} at large snowdepths:

$$\alpha = \alpha_0 + (\alpha_{sT} - \alpha_0)\left(1 - e^{-0.2\,\sigma}\right) \tag{76}$$

where σ is the lying snow in kg m^{-2}. This equation is intended to represent the combined effects of snowdepth, heterogeneity and masking on the surface albedo. The e folding depth is equivalent to 5mm of water. The deep-snow albedo has a simple temperature dependence for surface temperatures, T_*, above 2°C:

$$\alpha_{sT} = \begin{cases} \alpha_s & \text{for } T_* \le 2°C \\ \alpha_s + 0.15\,(\alpha_0 - \alpha_s)\,(T_* + 2) & \text{for } T_* > 2°C \end{cases} \tag{77}$$

where α_s is the cold deep-snow albedo appropriate to the surface. Values for α_0 and α_s are calculated as area-weighted means of the values specified for each surface type in the gridbox (see table 1).

When snow is lying the top two subsurface temperature layers are reinterpretetated as snow/soil layers. The insulating effect of snow cover is incorporated by modifying the surface thermal conductivity, λ, and the diffusive heat flux G_1 (see equation 34). In making these modifications the deeper subsurface temperatures are still treated as being at their usual positions below the soil surface, but the top subsurface temperature, T_{s1}, is taken to be $\Delta z_1/2$ below the surface whether snow is present or not. This temperature is therefore either within the snow or within the soil depending on the snow depth, Δz_{snow}, given by:

$$\Delta z_{snow} = \frac{\sigma}{\rho_{snow}} \tag{78}$$

where the snow density, ρ_{snow}, is fixed at 250 kg m^{-3}. The effective surface thermal conductivity, λ, is modified appropriately by treating the snow and soil as resistors in series:

$$\lambda = \begin{cases} \lambda_s \left\{ \dfrac{\Delta z_1}{\Delta z_1 + 2\,\Delta z_{snow}\,(\lambda_s/\lambda_{snow} - 1)} \right\} & \text{for } \Delta z_{snow} \le 0.5\,\Delta z_1 \\ \lambda_{snow} & \text{for } \Delta z_{snow} > 0.5\,\Delta z_1 \end{cases} \tag{79}$$

Here λ_s is the soil thermal conductivity as described in appendix B and λ_{snow} is the thermal conductivity of the snow, taken to be 0.265 W m^{-1} K^{-1}. The heat flux, G_1, from the first to the second subsurface temperature is modified to account for the increased separation between T_{s1} and T_{s2} when snow is present. When $\Delta z_{snow} > 0.5\,\Delta z_1$ this separation is partly snow and partly soil so the effective thermal conductivity must also be modified. The overall effect on G_1 is to reduce it by a multiplicative factor, ζ_1, given by:

$$\zeta_1 = \begin{cases} \dfrac{\Delta z_1 + \Delta z_2}{\Delta z_1 + \Delta z_2 + 2\,\Delta z_{snow}} & \text{for } \Delta z_{snow} \le 0.5\,\Delta z_1 \\ \dfrac{\Delta z_1 + \Delta z_2}{2\,\Delta z_1 + \Delta z_2 + \lambda_s/\lambda_{snow}\,\{2\,\Delta z_{snow} - \Delta z_1\}} & \text{for } \Delta z_{snow} > 0.5\,\Delta z_1 \end{cases} \tag{80}$$

The aerodynamic roughness associated with vegetation and very small scale irregularities (but not mountains) is also reduced in the presence of snow:

$$z_0 = z_{0v} - 4 \times 10^{-4}\,\sigma \tag{81}$$

where z_{0v} is the effective snow-free roughness length of the gridbox in metres, calculated as outlined in section 2f.

Land Class	d_r (m)	α_0	α_s	r_s (sm^{-1})	z_{0v} (m)	c_m (mm)	I_v	L	h (m)
Ice	0.0	0.75	0.8	0	0.0001	0.0	0	0	0.0
Inland Lake	1.0	0.06	0.8	0	0.0003	0.0	1	0	0.0
E N Tree	0.9	0.14	0.2	85	1.00	1.2	6	6	19.1
E B Tree	1.5	0.12	0.2	130	1.20	0.7	6	9	29.4
D N Tree	0.9	0.13	0.3	85	1.00	1.0	6	4	10.0
D B Tree	1.2	0.13	0.3	100	1.00	0.6	6	5	14.9
Tropical B Tree	1.5	0.13	0.2	130	1.20	0.7	6	9	29.4
D Drought Tree	0.9	0.13	0.3	100	1.00	0.6	4	5	14.9
E B Shrub	0.9	0.17	0.5	80	0.40	1.0	3	3	1.7
D Shrub	0.9	0.16	0.5	80	0.40	1.0	3	3	1.7
Thorn Shrub	0.6	0.16	0.5	80	0.40	1.0	3	2	1.4
Short Grass	0.5	0.19	0.7	60	0.01	0.5	1.5	2	0.4
Long Grass	0.7	0.20	0.6	80	0.04	0.7	2	4	0.8
Arable	0.7	0.20	0.8	60	0.04	0.5	2	5	1.0
Rice	0.8	0.12	0.7	40	0.01	0.7	2	5	1.0
Sugar	0.7	0.17	0.7	40	0.08	1.0	2	5	1.0
Maize	0.7	0.19	0.7	40	0.08	0.6	2	5	1.0
Cotton	0.7	0.19	0.7	35	0.10	0.8	2	5	1.0
Irrigated Crop	0.8	0.25	0.7	40	0.04	0.7	2	5	1.0
Urban	0.0	0.18	0.4	200	1.50	0.5	0.10	0	0.0
Tundra	0.25	0.15	0.8	40	0.01	0.7	1	1	1.0
Swamp	1.0	0.12	0.7	40	0.01	1.0	1	3	0.6
Soil	0.10		0.8	100	0.0003	0.5	0.5	0	0.0

Table 1: Surface parameters as specified for each of the Wilson and Henderson-Sellers land cover classes; rootdepth, d_r, snow-free albedo, α_0, cold deep-snow albedo, α_s, surface resistance, r_s, roughness length, z_{0v}, canopy water capacity, c_m, surface infiltration enhancement factor, I_v, leaf area index, L, and canopy height, h. The latter two parameters are only used by MOSES, whilst the rootdepth and surface resistance are only used directly by the UKMO scheme. The soil snow-free albedo is dependent on the soil colour as specified in the Wilson and Henderson-Sellers (1985) dataset and varies from 0.11 for dark soils to 0.35 for bright desert soils. Key: E - Evergreen; D - Deciduous; B - Broadleaf; N - Needleleaf.

Parameter	Soil Texture		
	Fine	Medium	Coarse
f_{sand}	0.21	0.27	0.58
f_{silt}	0.27	0.50	0.32
f_{clay}	0.52	0.23	0.10
b	11.20	6.63	4.50
K_s (mm s^{-1})	3.63×10^{-3}	4.72×10^{-3}	7.57×10^{-3}
Ψ_s (m)	4.53×10^{-2}	4.95×10^{-2}	3.29×10^{-2}
Θ_c	0.310	0.242	0.150
Θ_s	0.456	0.458	0.419
Θ_w	0.221	0.136	0.064
C_s (J K^{-1} m^{-3})	1.23×10^6	1.19×10^6	1.25×10^6
λ_{dry} (W m^{-1} K^{-1})	0.218	0.227	0.272

Table 2: Assumed particle-size fractions and calculated soil parameters for the 3 Wilson and Henderson-Sellers soil textural classes; fraction of sand, f_{sand}, fraction of silt, f_{silt}, fraction of clay, f_{clay}, Clapp-Hornberger exponent, b, saturated hydraulic conductivity, K_s, saturated soil water suction, Ψ_s, volumetric soil moisture concentrations at critical, saturation and wilting points, Θ_c, Θ_s and Θ_w respectively, dry soil volumetric heat capacity, C_s, and dry soil thermal conductivity, λ_{dry}. The wilting point and critical point are assumed to correspond to soil water suctions equivalent to 1.5 MPa and 0.033 MPa respectively.

	UKMO Scheme	MOSES
Surface Temperature	Prognostic - top soil layer	Diagnostic - from surface energy balance
Soil Characteristic Curves	van Genuchten	Clapp-Hornberger
Soil Hydraulic Parameters	area means	from area mean particle size distribution
Soil Thermal Parameters	constants	vary with soil water and ice content
Soil Water Phase Change	not included	by apparent heat capacity approach
Canopy Conductance	non-interactive	interactive and dependent on CO_2
Rootdepths	$\leq$1.5 metres, $\geq$0.5 metres	$\leq$3.0 metres, $\geq$1.0 metres
Surface CO_2 fluxes	not simulated	simulated

Table 3: Principle differences between the UKMO land surface scheme and MOSES

(a) 1×CO_2 UKMO

Variable	Mean Error				RMS Error			
	DJF	MAM	JJA	SON	DJF	MAM	JJA	SON
1.5m Temperature (K)	-3.08	-1.60	-0.20	-2.23	5.32	3.58	3.42	4.17
Precipitation (mm day^{-1})	-0.15	0.04	-0.15	-0.12	1.41	1.38	1.46	1.25

(b) 1×CO_2 MOSES

Variable	Mean Error				RMS Error			
	DJF	MAM	JJA	SON	DJF	MAM	JJA	SON
1.5m Temperature (K)	-2.57	-1.59	-0.62	-1.85	4.75	3.58	3.14	3.65
Precipitation (mm day^{-1})	-0.09	0.08	-0.04	-0.04	1.38	1.41	1.48	1.27

(c) 1×CO_2 MOSES without soil freezing

Variable	Mean Error				RMS Error			
	DJF	MAM	JJA	SON	DJF	MAM	JJA	SON
1.5m Temperature (K)	-3.00	-1.45	-0.24	-2.22	5.22	3.49	3.21	4.04
Precipitation (mm day^{-1})	-0.11	0.04	-0.04	-0.08	1.34	1.43	1.47	1.25

Table 4: Mean and RMS errors relative to the Legates and Willmott climatology for land points less than 1500 metres above sea-level. (a) 1×CO_2 UKMO run; (b) 1×CO_2 MOSES run; (c) 1×CO_2 MOSES run without soil freezing.

(a) UKMO

Variable	DJF	MAM	JJA	SON	Annual
1.5m Temperature (K)	3.48	3.09	2.97	3.19	3.18
Cloud Amount	0.00	-0.01	-0.02	-0.01	-0.01
Available Soil Moisture (mm)	0.05	-1.80	-5.31	-4.53	-2.90
Precipitation (mm day^{-1})	0.17	0.07	0.02	0.07	0.08
Evaporation (mm day^{-1})	0.06	0.11	0.05	0.02	0.06
Runoff (mm day^{-1})	0.05	0.04	0.02	0.01	0.02

(b) MOSES

Variable	DJF	MAM	JJA	SON	Annual
1.5m Temperature (K)	3.62	3.46	3.39	3.34	3.45
Cloud Amount	-0.01	-0.03	-0.04	-0.02	-0.03
Available Soil Moisture (mm)	6.08	7.56	-1.50	-0.27	2.97
Precipitation (mm day^{-1})	0.06	-0.03	-0.02	0.06	0.02
Evaporation (mm day^{-1})	-0.05	-0.03	-0.05	-0.08	-0.05
Runoff (mm day^{-1})	0.08	0.04	0.08	0.09	0.07

(c) MOSES without soil freezing

Variable	DJF	MAM	JJA	SON	Annual
1.5m Temperature (K)	3.67	3.32	3.18	3.53	3.43
Cloud Amount	-0.01	-0.02	-0.04	-0.02	-0.02
Available Soil Moisture (mm)	2.66	2.63	-3.05	-2.19	0.01
Precipitation (mm day^{-1})	0.09	0.01	-0.02	0.04	0.03
Evaporation (mm day^{-1})	-0.03	-0.01	-0.05	-0.08	-0.05
Runoff (mm day^{-1})	0.09	0.07	0.08	0.07	0.08

(d) MOSES without direct CO_2 effect

Variable	DJF	MAM	JJA	SON	Annual
1.5m Temperature (K)	3.37	3.01	2.78	3.08	3.06
Cloud Amount	0.00	-0.01	-0.02	-0.01	-0.01
Available Soil Moisture (mm)	3.13	4.63	-4.55	-3.75	-0.14
Precipitation (mm day^{-1})	0.11	0.03	0.02	0.04	0.05
Evaporation (mm day^{-1})	0.02	0.05	0.03	-0.03	0.02
Runoff (mm day^{-1})	0.05	0.01	0.05	0.04	0.03

Table 5: Sensitivity of the climate over land to doubling CO_2. (a) UKMO; (b) MOSES; (c) MOSES without soil freezing; (d) MOSES without direct CO_2 effect.

(a) 1× CO_2 MOSES

Variable	DJF	MAM	JJA	SON	Annual
Canopy Conductance (mm s^{-1})	2.08	2.98	4.26	2.52	2.96
Gross Primary Productivity (kg C m^{-2} yr^{-1})	0.71	0.94	1.27	0.83	0.94
Net Primary Productivity (kg C m^{-2} yr^{-1})	0.32	0.45	0.62	0.36	0.44
Plant Respiration (kg C m^{-2} yr^{-1})	0.39	0.49	0.65	0.47	0.50

(b) 2× CO_2 MOSES

Variable	DJF	MAM	JJA	SON	Annual
Canopy Conductance (mm s^{-1})	1.24	1.83	2.46	1.44	1.74
Gross Primary Productivity (kg C m^{-2} yr^{-1})	0.96	1.31	1.68	1.07	1.25
Net Primary Productivity (kg C m^{-2} yr^{-1})	0.47	0.69	0.89	0.51	0.64
Plant Respiration (kg C m^{-2} yr^{-1})	0.49	0.62	0.79	0.56	0.61

(b) 2× CO_2 MOSES without direct CO_2 effect

Variable	DJF	MAM	JJA	SON	Annual
Canopy Conductance (mm s^{-1})	2.02	3.08	4.12	2.33	2.89
Gross Primary Productivity (kg C m^{-2} yr^{-1})	0.68	0.95	1.21	0.75	0.90
Net Primary Productivity (kg C m^{-2} yr^{-1})	0.27	0.42	0.54	0.28	0.38
Plant Respiration (kg C m^{-2} yr^{-1})	0.41	0.53	0.66	0.47	0.52

Table 6: Canopy conductance and carbon fluxes as simulated by MOSES. (a) 1×CO_2; (b) 2×CO_2; (c) 2×CO_2 without the direct CO_2 effect on vegetation.

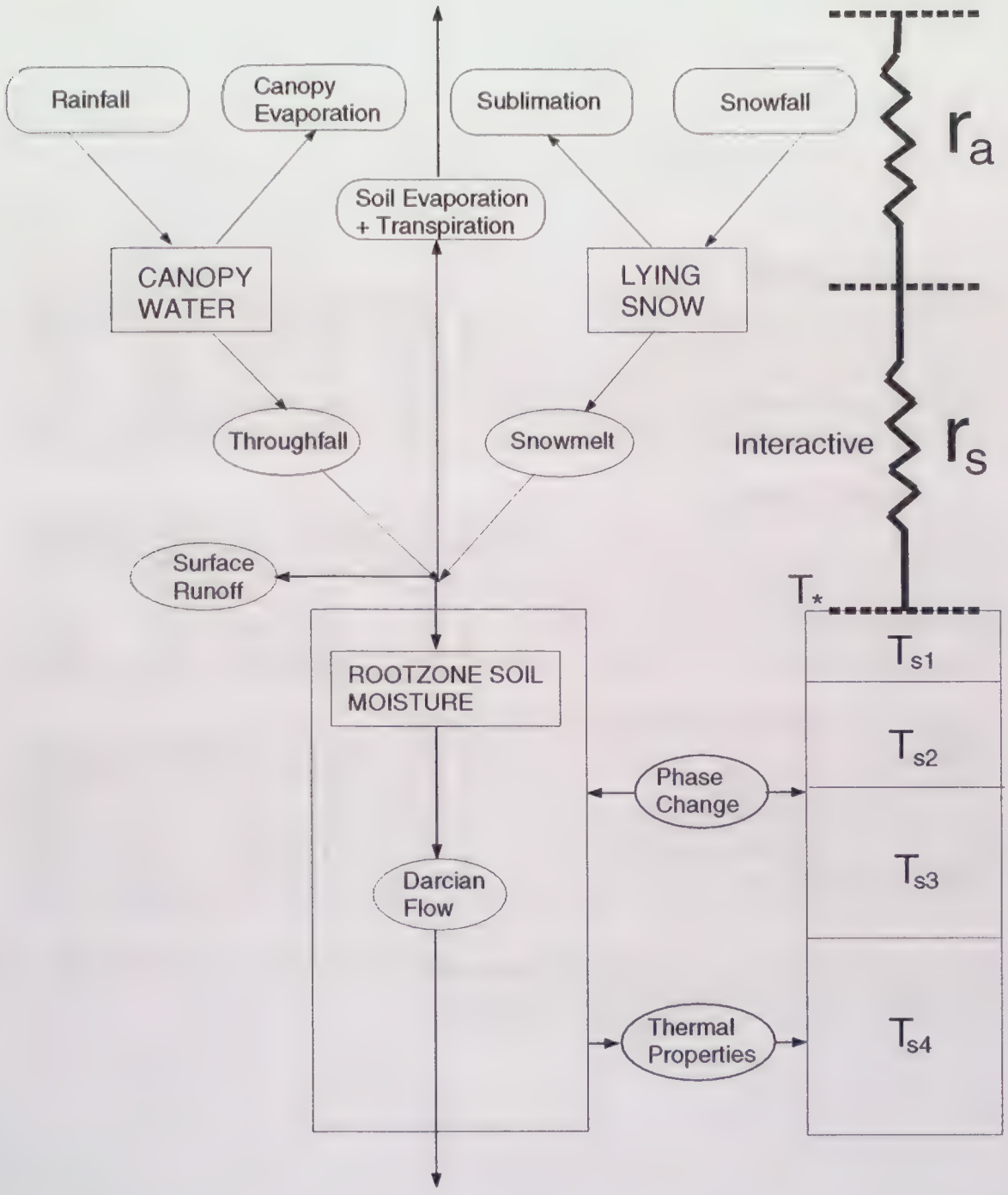

Figure 1: Schematic representation of the Met Office Surface Exchange Scheme (MOSES). Prognostic variables are denoted by rectangles. Note the main new features which have been introduced; a "skin" surface temperature (T_*), an interactive surface resistance (r_s) and the inclusion of soil water phase change effects.

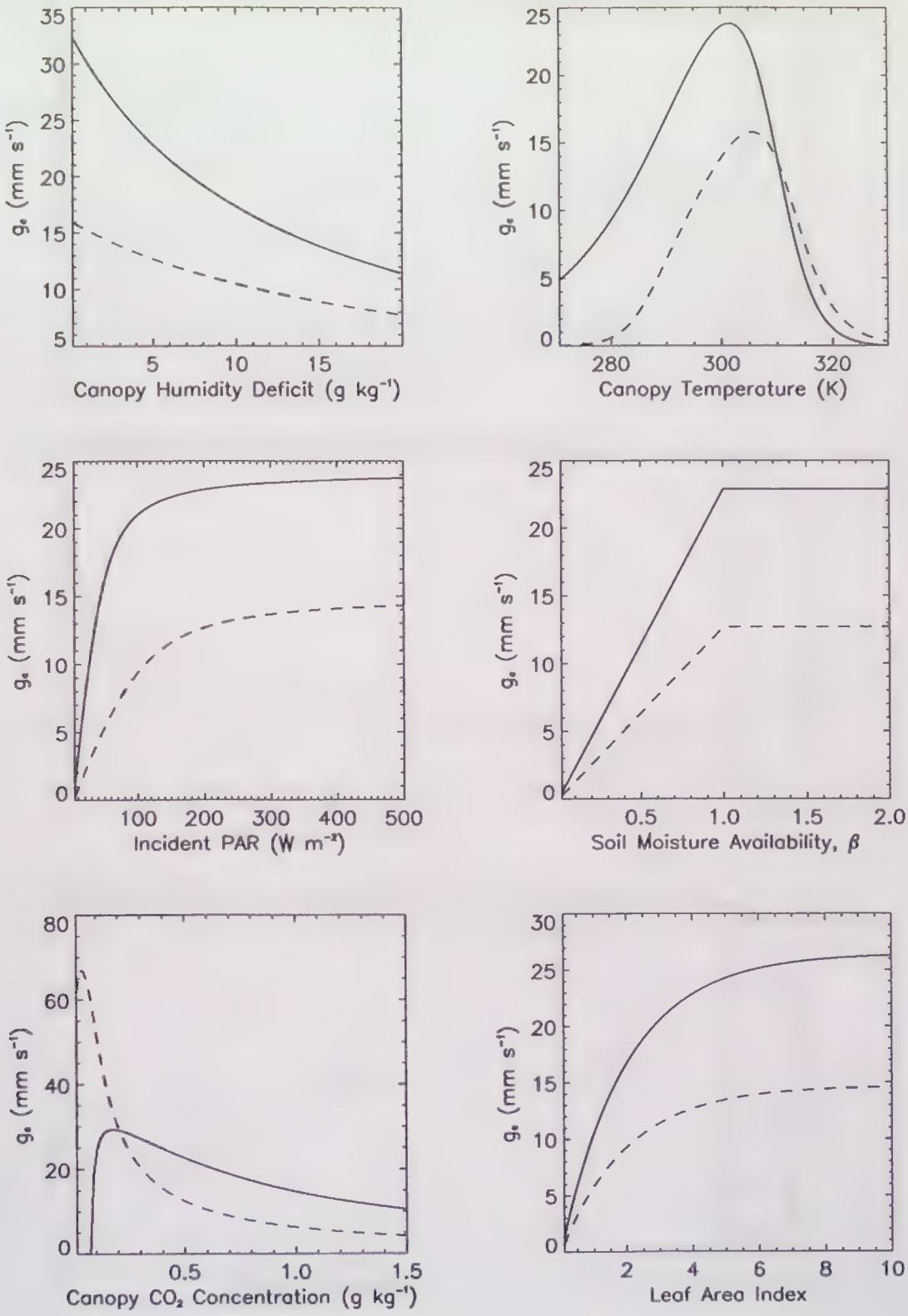

Figure 2: Dependences of the MOSES canopy conductance on environmental and structural variables. Typical responses of C_3 and C_4 grasses are represented by the continuous and dotted lines respectively. (Defaults : $dq = 5.0$ g kg^{-1}, $T = 298.15$ K, $\beta = 1.0$, $PAR = 200$ W m^{-2}, CO_2=0.490 g kg^{-1}, LAI=4.0).

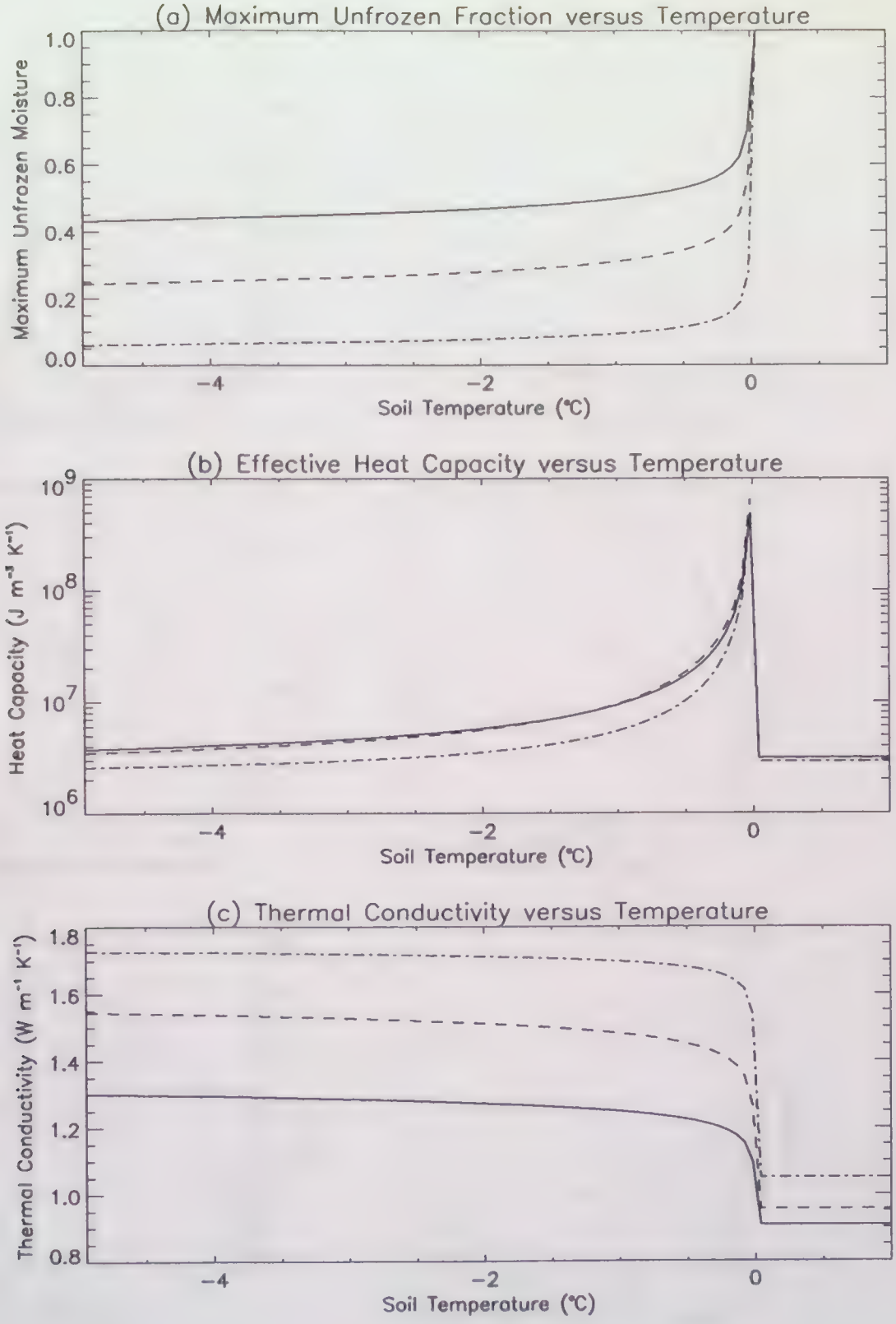

Figure 3: (a) Maximum unfrozen soil moisture as a fraction of saturation, (b) effective heat capacity and (c) thermal conductivity versus soil temperature for the three soil textures used in MOSES: fine (continuous line), medium (dashed line) and coarse (dot-dash line).

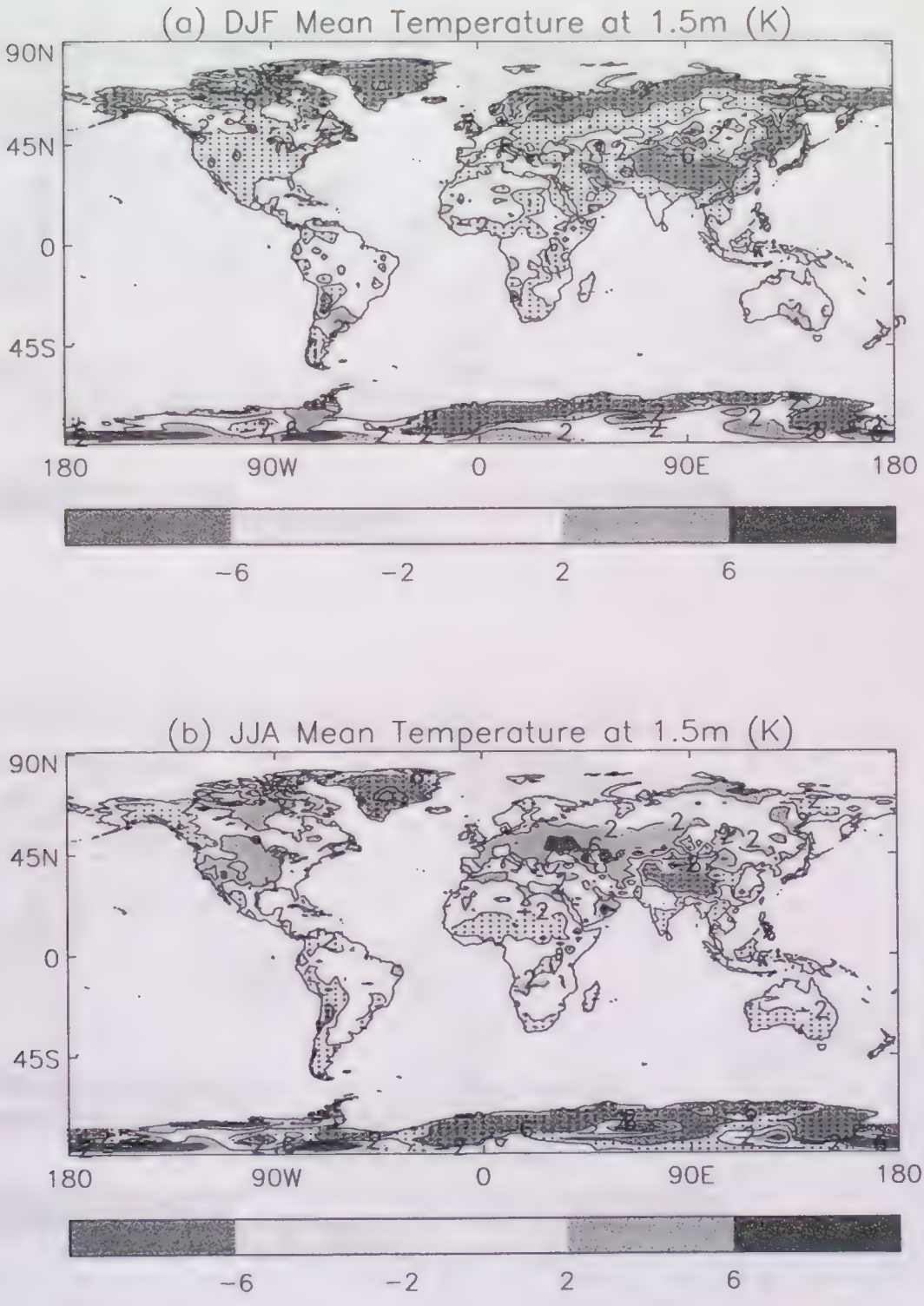

Figure 4: Errors in mean screen level temperature for (a) December-January-February and (b) June-July-August relative to the Legates and Willmott climatology, for the control simulation using the UKMO land surface scheme. Values below -2 are indicated by the heavy dots.

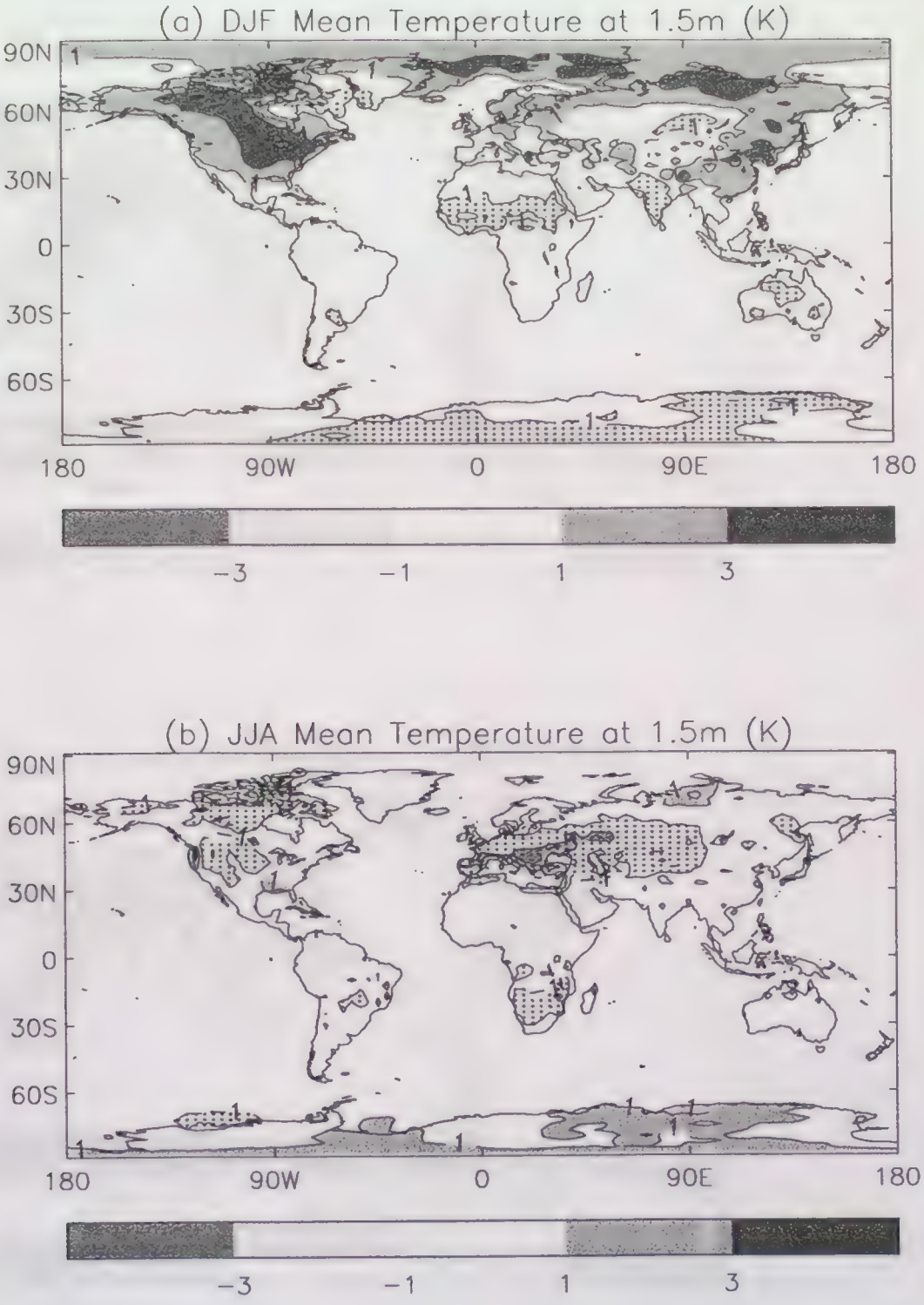

Figure 5: Impact of MOSES on the simulated mean screen level temperatures for (a) December-January-February and (b) June-July-August, calculated as the difference between the simulations using MOSES and UKMO. Values below -1 are indicated by heavy dots. Note the different scale compared to Figure 4.

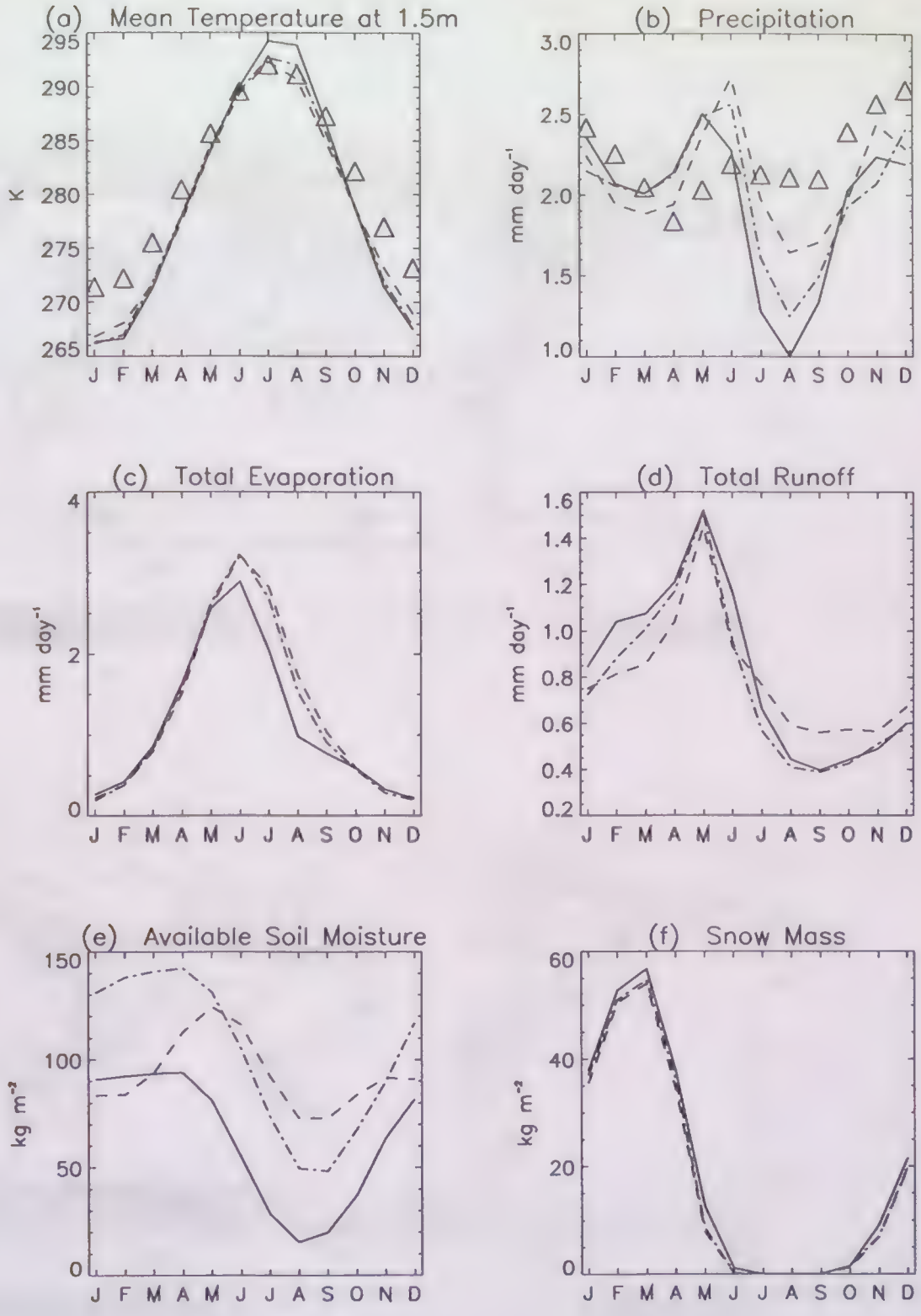

Figure 6: Simulation of the climate over European land (20°W-40°E, 35°N-75°N) for the simulations using UKMO (continuous line), MOSES (dashed line), and MOSES excluding the effects of soil freezing (dot-dashed line). The symbols represent the means as given by the Legates and Willmott climatology. Screen level temperature (a); precipitation (b); total evaporation (c); total runoff (d); available soil moisture (e) and snow mass (f).

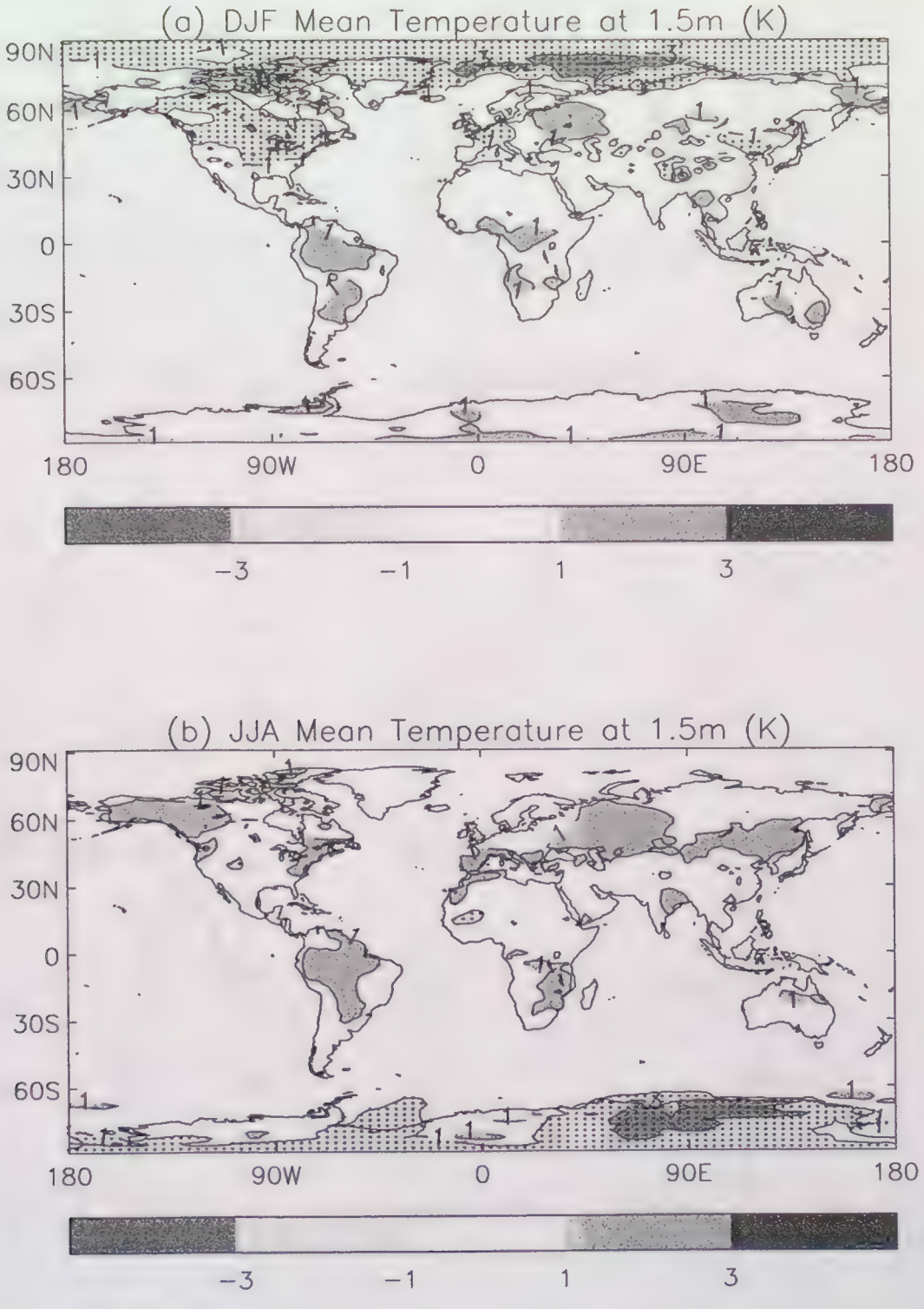

Figure 7: Impact of MOSES on the sensitivity of screen-level temperature to doubling CO_2 for (a) December-January-February and (b) June-July-August. Calculated by subtracting the UKMO climate sensitivity from the MOSES climate senstivity. Values below -1 are indicated by heavy dots.

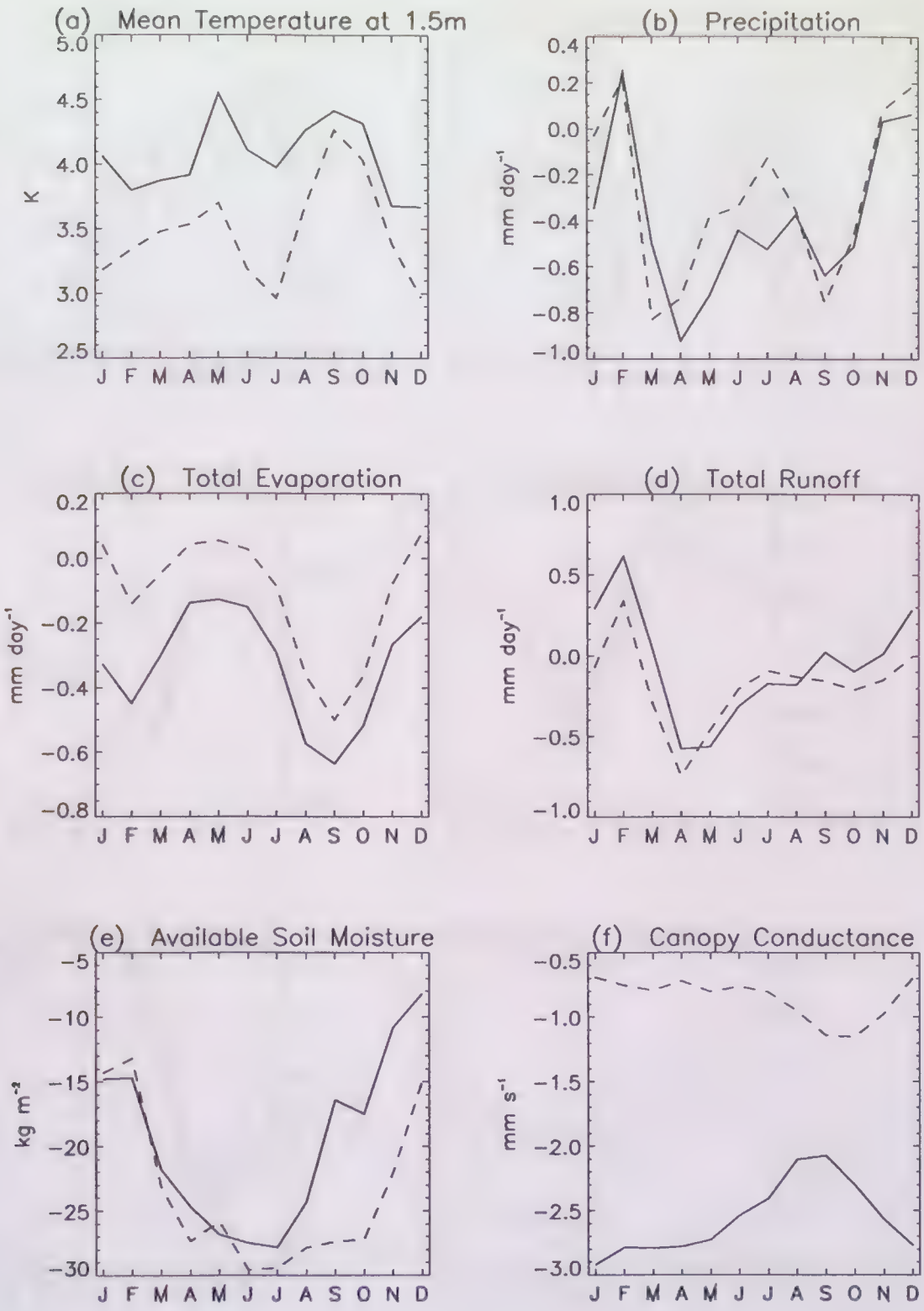

Figure 8: Sensitivity of the climate over Amazonian land (90°W-30°W, 30°S-10°N) to doubling CO_2, from the simulations using MOSES (continuous line), and MOSES without the direct CO_2 effect (dashed line). Screen level temperature (a); precipitation (b); total evaporation (c); total runoff (d); available soil moisture (e) and canopy conductance (f).

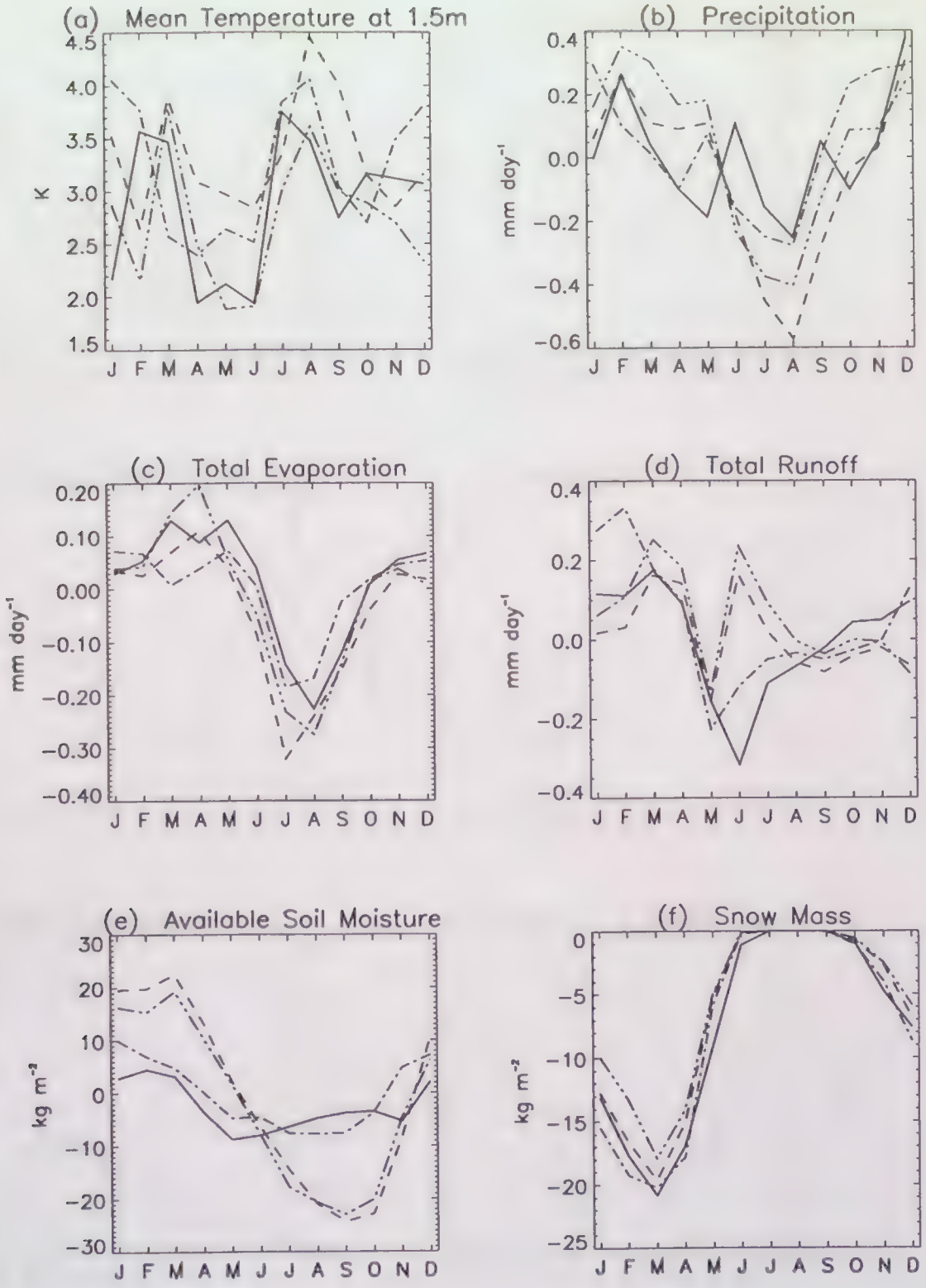

Figure 9: Sensitivity of the climate over European land to doubling CO_2, from the simulations using UKMO (continuous line), MOSES (dashed line), MOSES without soil freezing (dot-dash line) and MOSES without the direct CO_2 effect (dot-dot-dot-dash line). Screen level temperature (a); precipitation (b); total evaporation (c); total runoff (d); available soil moisture (e) and snow mass (f).

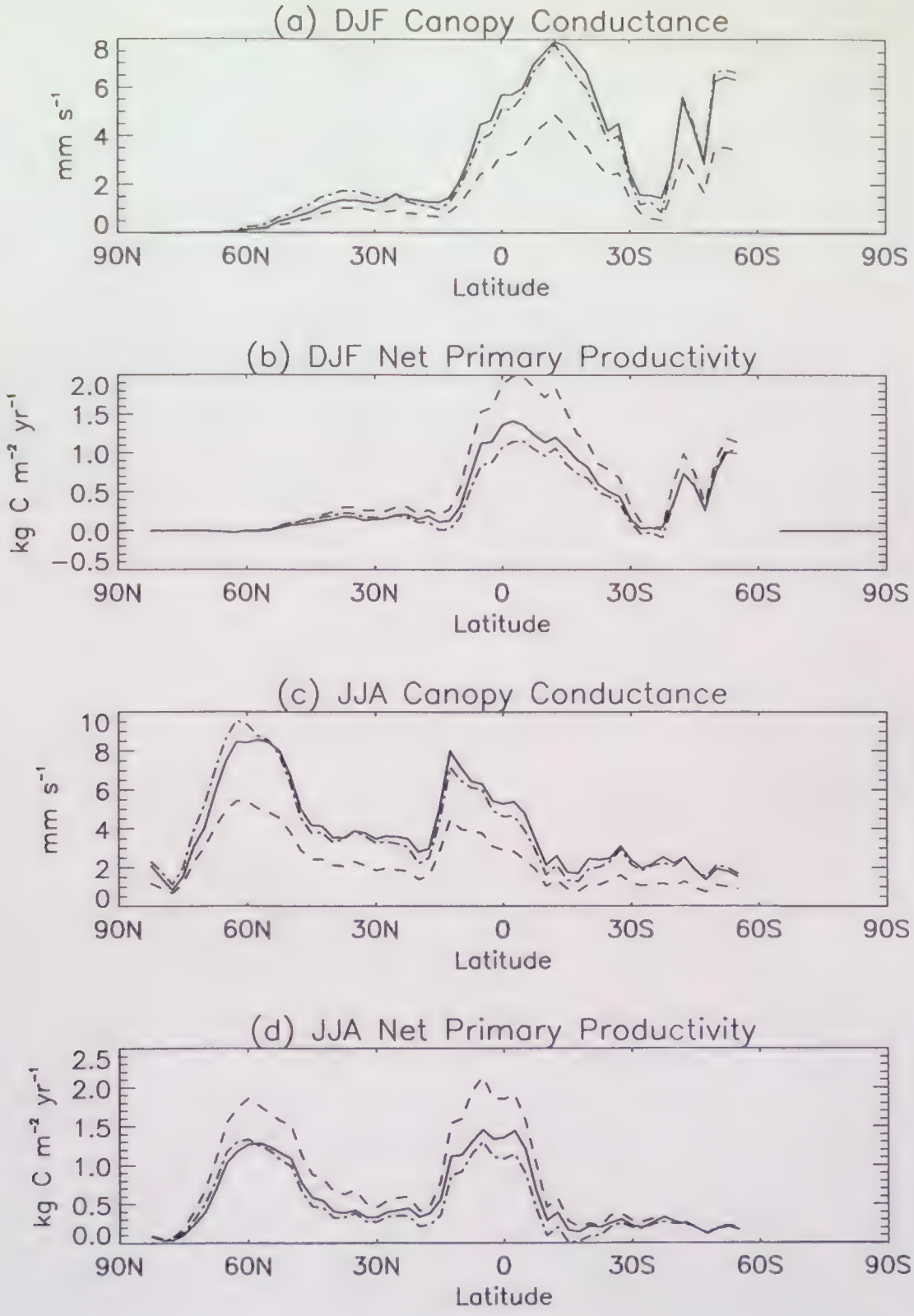

Figure 10: Zonal mean canopy conductance and net primary productivity over land from the $1\times CO_2$ MOSES simulation (continuous line), the $2\times CO_2$ MOSES simulation (dash line) and the $2\times CO_2$ MOSES simulation without the direct CO_2 effect on vegetation (dot-dash line). DJF canopy conductance (a); DJF net primary productivity (b); JJA canopy conductance (c) and JJA net primary productivity (d).

CLIMATE RESEARCH TECHNICAL NOTES

CRTN 1	Oct 1990	Estimates of the sensitivity of climate to vegetation changes using the Penman-Monteith equation. P R Rowntree
CRTN 2	Oct 1990	An ocean general circulation model of the Indian Ocean for hindcasting studies. D J Carrington
CRTN 3	Oct 1990	Simulation of the tropical diurnal cycle in a climate model. D P Rowell
CRTN 4	Oct 1990	Low frequency variability of the oceans. C K Folland, A Colman, D E Parker and A Bevan
CRTN 5	Dec 1990	A comparison of 11-level General Circulation Model Simulations with observations in the East Sahel. K Maskell
CRTN 6	Dec 1990	Climate Change Prediction. J F B Mitchell and Qing-cun Zeng
CRTN 7	Jan 1991	Deforestation of Amazonia - modelling the effects of albedo change. M F Mylne and P R Rowntree
CRTN 8	Jan 1991	The role of observations in climate prediction and research. D J Carson
CRTN 9	Mar 1991	The greenhouse effect and its likely consequences for climate change. D J Carson
CRTN 10	Apr 1991	Use of wind stresses from operational N.W.P. models to force an O.G.C.M. of the Indian Ocean. D J Carrington
CRTN 11	Jun 1991	A new daily Central England Temperature series, 1772-1991. D E Parker, T P Legg and C K Folland
CRTN 12	Jul 1991	Causes and predictability of Sahel rainfall variability. D P Rowell, C K Folland, K Maskell, J A Owen, M N Ward

CLIMATE RESEARCH TECHNICAL NOTES

CRTN 13	Jul 1991	Modelling changes in climate due to enhanced CO2, the role of atmospheric dynamics, cloud and moisture. C A Senior, J F B Mitchell, H Le Treut and Z-X Li
CRTN 14	Sep 1991	Sea temperature bucket models used to correct historical SST data in the Meteorological Office. C K Folland
CRTN 15	Aug 1991	Modelling climate change, and some potential effects on agriculture in the U.K. P R Rowntree, B A Callander and J Cochrane
CRTN 16	Aug 1991	The Boreal Forests and Climate G Thomas and P R Rowntree
CRTN 17	Aug 1991	Development of a Stratosphere-Troposphere Data Assimilation System. R Swinbank.
CRTN 18	Sep 1991	A study of asynchronous coupling using a simple climate model. M K Davey.
CRTN 19	Sep 1991	The Oceanic Carbon Cycle. N K Taylor
CRTN 20	Nov 1991	Worldwide ocean-atmosphere surface fields in Sahel wet and dry years using provisionally corrected surface wind data. M N Ward
CRTN 21	Dec 1991	Coupled tropical ocean global atmosphere models at the UKMO. M K Davey, C Gordon, S Ineson and S Lawrence
CRTN 22	Dec 1991	Empirical parameterisation of tropical ocean-atmosphere coupling. M Allen, M K Davey, D L T Anderson and P D Killworth
CRTN 23	Feb 1992	The temporal evolution of Equatorial Currents in the Indian Ocean D L T Anderson, D J Carrington, R A Corry and C Gordon
CRTN 24	Feb 1992	Stratospheric analyses provided by the U.K. Meteorological Office M J Bailey, A O'Neill and V D Pope

CLIMATE RESEARCH TECHNICAL NOTES

CRTN 25	Feb 1992	Modelling interannual variability in the Indian Ocean using momentum fluxes from the UKMO and ECMWF operational weather analyses. D L T Anderson and D J Carrington
CRTN 26	Mar 1992	A GCM simulation of the impact of Amazonian deforestation on climate using an improved canopy representation J Lean and P R Rowntree
CRTN 27	Mar 1992	The parameterization of rainfall interception in GCMs A J Dolman and D Gregory
CRTN 28	Jun 1992	Development of worldwide marine data eigenvectors since 1985 A W Colman
CRTN 29	Jun 1992	A tropical ocean model with reduced physics M K Davey
CRTN 30	Jun 1992	International Temperature Workshop, Boulder, Colorado, USA, 16 January 1992 Edited by D E Parker
CRTN 31	Jul 1992	Simulation of clear-sky outgoing longwave radiation over the oceans using operational analyses A Slingo and M J Webb
CRTN 32	Sep 1992	A prediction of the transient response of climate J M Murphy
CRTN 33	Nov 1992	LEPS scores for assessing climate model simulations and long-range forecasts. C K Folland
CRTN 34	Jan 1993	Stratospheric Data Assimilation System Guide Editer: R Swinbank
CRTN 35	Mar 1993	A Stratosphere-Troposphere Data Assimilation System R Swinbank and A O'Neill
CRTN 36	Mar 1993	Validation of hydrological schemes for climate models against catchment data. P R Rowntree and J Lean

CLIMATE RESEARCH TECHNICAL NOTES

CRTN 37	Apr 1993	Modelling of palaeoclimates: Examples from the recent past J F B Mitchell
CRTN 38	May 1993	A simulation of seasonality in ENSO forecast skill M K Davey, D L T Anderson and S Lawrence
CRTN 39	Jul 1993	ENSO Prediction experiments using a simple ocean-atmosphere model D-H Wu, D L T Anderson and M K Davey
CRTN 40	Sep 1993	Diagnosis of dynamic sea-surface and sea-level changes from the Cox ocean model J M Gregory
CRTN 41	Sep 1993	Seasonal variations of the clear-sky greenhouse effect: the role of changes in atmospheric temperatures and humidities M J Webb, A Slingo and G L Stephens
CRTN 42	Nov 1993	Sea-level changes under increasing atmospheric CO_2 in a transient coupled ocean-atmosphere GCM experiment. J M Gregory
CRTN 43	Dec 1993	Global and regional patterns of climate change: recent predictions for the Arctic P R Rowntree
CRTN 44	Feb 1994	The effect of changing horizontal diffusion in the atmospheric version of the unified climate model C D Hall and R A Stratton
CRTN 45	Mar 1994	Simulation of El-Niño/Southern Oscillation like variability in a global AOGCM and its response to CO_2 increase. S F B Tett
CRTN 46	Apr 1994	Global data required for monitoring climate change. D E Parker and C K Folland
CRTN 47	May 1994	Seasonal uptake of anthropogenic CO_2 in an ocean general circulation model. N K Taylor

CLIMATE RESEARCH TECHNICAL NOTES

CRTN 48	Jun 1994	A tropic-wide oscillation of boreal summer rainfall and patterns of sea-surface temperature. M N Ward, K Maskell, C K Folland, D P Rowell and R Washington
CRTN 49	Jun 1994	Simulation of the tropical Pacific using a simplified ocean model M A Balmaseda, D L T Anderson and M K Davey
CRTN 50	Sep 1994	Simulation of global mean temperature using a box-diffusion climate model P R Rowntree
CRTN 51	Sep 1994	Seasonal dependence of ENSO prediction skill M A Balmaseda, M K Davey and D L T Anderson
CRTN 52	Nov 1994	Simulation of the Indian Monsoon and Tropical Intraseasonal Variability by a General Circulation Model P M Inness and D Gregory
CRTN 53	Mar 1995	A comparison of modelled surface fluxes with climatological estimates. C Gordon and D K Wright
CRTN 54	Mar 1995	The representation of moist convection in atmospheric models. D Gregory
CRTN 55	Mar 1995	A consistent treatment of the evaporation of rain and snow for use in large-scale models D Gregory
CRTN 56	Apr 1995	Workshop on simulations of the Climate of the Twentieth Century using GISST, 28-30 November 1994, Hadley Centre, Bracknell, UK Edited by C K Folland and D P Rowell
CRTN 57	May 1995	Enhanced shortwave cloud radiative forcing due to anthropogenic aerosols. S E Swartz and A Slingo
CRTN 58	May 1995	The simulation of the tropical oceans in models of different horizontal resolution. C Gordon, D K Wright and C M Roberts
CRTN 59	Sep 1995	The water budget of middle latitude continental regions - a modelling and observational study P R Rowntree
CRTN 60	Sep 1995	Intraseasonal variability of the Indian summer monsoon simulated by the Hadley Centre climate model K Ashok, D Gregory and P M Inness

CLIMATE RESEARCH TECHNICAL NOTES

CRTN 61	Sep 1995	Climate simulations with the Unified Model: AMIP runs C D Hall, R A Stratton and M L Gallani
CRTN 62	Nov 1995	Validation of surface parameters over the oceans in climate simulations with the unified model. C D Hall
CRTN 63	Dec 1995	The GISST2.2 sea surface temperature and sea-ice climatology D E Parker, M Jackson and E B Horton
CRTN 64	Dec 1995	Parametrization of momentum transport by convection. II: Tests in single column and general circulation models. D Gregory, R Kershaw and P M Inness
CRTN 65	Jan 1996	Understanding the sensitivity of a GCM simulation of Amazonian deforestation to the specification of vegetation and soil characteristics. J Lean and P R Rowntree
CRTN 66	Jan 1996	On the efficient calculation of infra-red fluxes and cooling rates using the two-stream equations. J M Edwards
CRTN 67	Jan 1996	The second Hadley Centre coupled ocean-atmosphere GCM: Model description, spinup and validation. TC Johns,RE Carnell,JF Crossley,JM Gregory, JFB Mitchell,CA Senior,SFB Tett and RA Wood
CRTN 68	Feb 1996	The sensitivity of climate simulations to the specification of mixed phase clouds D Gregory and D Morris
CRTN 69	Apr 1996	Using an ensemble of Multi-Decadal GCM simulations ro assess potential seasonal predictability D P Rowell
CRTN 70	May 1996	North Atlantic and European Seasonal Predictability using an Ensemble of Multi-Decadal AGCM Simulations J R Davies, D P Rowell and C K Folland
CRTN 71	Jun 1996	A description of the Second Hadley Centre Coupled Model (HADCM2) T C Johns
CRTN 72	Jul 1996	Palaeoclimate Modelling Intercomparison: UKMO GCM simulations for 6kBP and 21kBP C D Hewitt and J F B Mitchell

CLIMATE RESEARCH TECHNICAL NOTES

CRTN 73	Aug 1996	ENSO responses and low frequency weather variability in the North Pacific/American sector 1949-93 A C Renshaw, D P Rowell and C K Folland
CRTN 74	Sep 1996	Version 2.2 of the Global sea-Ice and Sea Surface Temperature data set, 1903-1994 N A Rayner, E B Horton, D E Parker, C K Folland and R B Hackett
CRTN 75	Sep 1996	A new gravity wave drag scheme incorporating anisotropic orography and low level wave breaking : Impact upon the climate of the UK Met Office Unified Model D Gregory, G J Shutts and J R Mitchell
CRTN 76	Nov 1996	Middle atmosphere variability in the UKMO Unified Model R Swinbank, W Lahoz, C Douglas, A Heaps, R Brugge, W Norton, A O'Neill, D Podd
CRTN 77	Dec 1996	A high resolution AMIP run using the Hadley Centre model HadAM2b R A Stratton
CRTN 78	Jan 1997	The climate response to CO_2 of the Hadley Centre coupled AOGCM with and without flux adjustment J M Gregory and J F B Mitchell
CRTN 79	May 1997	Development of the Global Mean Sea Level Pressure Data Set GMSLP2 T A Basnett and D E Parker
CRTN 80	Jun 1997	Seasonal Forecasting D J Carson
CRTN 81	Feb 1998	Large scale modes of ocean surface temperature since the late nineteenth century C K Folland, D E Parker, A W Colman and R Washington
CRTN 82	Mar 1998	The impact of new land surface physics on the GCM simulation of climate and climate sensitivity. P M Cox, R A Betts, C B Bunton, R L H Essery, P R Rowntree and J Smith